5-2015

Terrestrial Impacts of the Central Atlantic Magmatic Province on western Pangea

Todd Kenneth Knobbe
University of Arkansas, Fayetteville

Terrestrial Impacts of the Central Atlantic Magmatic Province on western Pangea

Terrestrial Impacts of the Central Atlantic Magmatic Province on western Pangea

A thesis submitted in partial fulfillment
of the requirements for the degree of
Master of Science in Geology

by

Todd Knobbe
University of Arkansas
Bachelor of Science in Geology, 2013

May 2015
University of Arkansas

This thesis is approved for recommendation to the Graduate Council.

Dr. Celina Suarez
Thesis Director

Dr. Phillip Hays
Committee Member

Dr. Doy Zachry
Committee Member

ABSTRACT

Earth's climate is predominantly controlled by the fluctuation of greenhouse gases, specifically CO_2 and CH_4, over geologic time. The late Triassic is a period of abrupt climate change that has been associated with a disruption to the global carbon cycle due the emplacement of the Central Atlantic Magmatic Province (CAMP). Evidence has shown that this global carbon cycle perturbation may be the culprit for the end-Triassic extinction. The Whitmore Point Member of the Moenave Formation is a lacustrine deposit with a disputed age of either late Triassic or early Jurassic and currently no absolute dating techniques can be applied to estimate an exact age. Therefore, I propose that identification of the CAMP carbon cycle perturbation through carbon isotope chemostratigraphy of the Whitmore Point Member will be the best current age constraint. $\delta^{13}C_{organic}$ and $\delta^{13}C_{carbonate}$ were analyzed in the lacustrine deposits of the Whitmore Point Member of the Moenave Formation to construct a carbon isotope chemostratigraphic profile. Carbon isotope evidence indicates that the environmental perturbation caused by the emplacement of the CAMP is present within the Whitmore Point Member. Data was collected at two localities: 1) The Whitmore Point Reference Section (Potter Canyon, Arizona) and 2) Warner Valley, Utah. Carbon isotope data from Potter Canyon reveals a distinctive 5.5‰ and 2.75‰ decrease in $\delta^{13}C_{organic}$ and $\delta^{13}C_{carbonate}$, respectively, in the lower portion of the Whitmore Point Member. Warner Valley does not show a prominent negative carbon isotope excursion but has been correlated to the positive isotope excursion and main negative isotope excursion exhibited within Potter Canyon. Correlation of carbon isotope curves from different localities also helps to regionally correlate the Whitmore Point Member. The identification of the Potter Canyon negative carbon isotope excursion is the first terrestrial record of the CAMP in western Pangea and provides more compelling evidence on the global impacts of the CAMP. Carbon isotope data along with previously published conchostracan data indicates

that the end-Triassic extinction is within the lower portion of the Whitmore Point Member while the Triassic – Jurassic boundary is present within the upper portion. Therefore, I propose the age of the Whitmore Point Member to be late Triassic to early Jurassic.

ACKNOWLEDGEMENTS

I would like to thank Dr. Celina Suarez for all of her patience, support, advice, and willingness to help me succeed in this endeavor. I would also like to thank my committee members for their help and support throughout my time as a student at the University of Arkansas. Their educational guidance has been greatly appreciated. A special thanks goes out to the Erik Pollock and Lindsay Conaway at the University of Arkansas Stable Isotope Lab. Thanks goes to Dr. Jim Kirkland, Andrew Milner, and Dr. Marina Suarez for aiding with sample collection and field work. Their knowledge of the Moenave Formation has greatly aided me in my research. Special thanks goes to the Bureau of Land Management for granting me permission to work on BLM land. Thanks also goes to the Geological Society of America Graduate Research Grants for partially funding this research. I greatly appreciate all the professors in the University of Arkansas Department of Geosciences whom have inspired me to study different aspects of geology. Lastly, appreciation goes out to my family and friends who have supported, motivated and encouraged me over the past two years.

TABLE OF CONTENTS

I. INTRODUCTION……...……....1
II. BACKGROUND……..……...…4
A. CARBON ISOTOPE CHEMOSTRATIGRAPHY……...4
B. ORGANIC AND INORGANIC CARBON ISOTOPE FRACTIONATION……...…8
C. EFFECTS OF DIAGENESIS ON CARBON ISOTOPES……..14
D. CENTRAL ATLANTIC MAGMATIC PROVINCE……...…16
E. END-TRIASSIC EXTINCTION……19
F. TRIASSIC – JURASSIC BOUNDARY……..22
G. MOENAVE FORMATION……23
1. STRATIGRAPHY…...…….....23
2. LITHOLOGY……24
3. BIOSTRATIGRAPHY……...27
III. CASE STUDY……...29
A. INTRODUCTION……...29
B. GEOLOGIC SETTING……..…….……33
C. STABLE ISOTOPE GEOCHEMISTRY METHODS……35
D. RESULTS……37
E. DISCUSSION…….…..…….……..……..……..……..…41
F. IMPLICATIONS…….…….…….…..48
IV. CONCLUSIONS…….…….…….…….…….…….....49
V. REFERENCES…….…….…….…….…….……..……..51
VI. APPENDIX…….……...58

LIST OF FIGURES

FIGURE		PAGE
1	SAMPLE LOCATIONS……	4
2	GLOBAL CARBON CYCLE……	7
3	CARBON ISOTOPE COMPOSITIONS……...	10
4	BJERRUM PLOT……..	12
5	LACUSTRINE CARBON ISOTOPES…….	14
6	CENTRAL ATLANTIC MAGMATIC PROVINCE……	17
7	TR-J GLOBAL CARBON ISOTOPE STRATIGRAPHY……	19
8	LIP AND EXTINCTION CORRELATION……..	20
9	GENERAL STRATIGRAPHIC SECTION AND PALEOGEOGRAPHY..	24
10	WPM HYPOTHETICAL STRATIGRAPHIC SECTION……	26
11	WPM SAMPLE LOCATIONS…….……..……	33
12	WPM CHEMOSTRATIGRAPHY……	38
13	$\delta^{13}C_{organic}$ VS. RELATIVE-TOTAL ORGANIC CARBON (%)…..……....	40
14	TR-J GLOBAL CARBON ISOTOPE STRATIGRAPHY……	42
15	WPM GLOBAL CORRELATION……	43

I. INTRODUCTION

The Earth system over geologic time has responded to various types of external forcings (volcanic, solar and orbital) and to changes in its atmospheric composition (Masson-Delmotte et al 2013). Climate change has been documented throughout Earth's history by numerous proxy methods (pedogenic carbonates, plant stomata, boron isotopes, alkenones etc.). Transitions from past climates have been recorded on the decadal, centennial and millennial levels (Masson-Delmotte et al 2013). Findings documented in the 2013 Intergovernmental Panel on Climate Change report have shown that external forcings (volcanic, solar and orbital) are contributing less to current climate change than anthropogenic forcings (fossil fuel emissions, cement production and land-use change). Anthropogenic forcing in the form of atmospheric CO_2 concentrations during the Industrial Era have increased by 40% (278 ppm to 390.5 ppm) from 1750 to 2011 while CH_4 concentrations have increased by 150% (722 ppb to 1803 ppb) during the same time interval (Ciasis et al 2013).

Models predict that estimated emissions of ~3.67 trillion tonnes of CO_2 into the atmosphere from fossil fuels will result in a 2°C increase in global temperatures (Allen et al 2009). Massive amounts of CO_2 injected into the atmosphere during a relatively short period of time can have devastating environmental effects (Bond and Wignall, 2014). Simulations estimate that atmospheric CO_2 concentrations can exceed 1,900 ppm which would lower ocean-surface pH by 0.77 affecting both biotic and abiotic carbonate precipitation (Caldeira and Wickett 2003). Ocean pH is relatively sensitive to CO_2 changes over short periods of time ($< 10^4$ years) while less sensitive to CO_2 changes over longer periods of time ($>10^5$ years) because carbonate minerals act as a buffer to massive CO_2 inputs; therefore, reducing sensitivity to pH change (Caldeira and Wickett 2003). Paleo-proxy methods (geochemistry of paleosols, foraminifera and

plant stomata) have shown that atmospheric CO_2 concentrations over the Phanerozoic have constantly fluxed between a minimum of 100 ppm and a maximum of 7,500 ppm (Caldeira and Wickett 2003). Modeling and future projections of current climate change have shown the effects of abrupt, anthropogenically induced climate change on the Earth system. Effects from anthropogenic activities will ultimately lead to a change in global climate, global temperature, ocean chemistry, and global biodiversity (Allen et al., 2009; Caldeira and Wickett 2003; Sala et al., 2000). While some of these figures seem staggering and beyond what we as human can conceptualize, similar changes have taken place in the geologic past.

Understanding past geologic events that are coupled to abrupt climate change and mass extinctions can provide key information on the cause and effect relationship between evolutionary responses to abrupt climate change as well as biotic response to modern rapid climate change. During the Phanerozoic, four major mass extinction events have been shown to coincide with the emplacement of large igneous provinces (LIPs) (Bond and Wignall 2014). Earth's climate has been shown to be controlled over geologic time by the flux of atmospheric gases, specifically the greenhouse gases carbon dioxide (CO_2) and methane (CH_4) (Cotton and Sheldon 2012). The release of volcanogenic CO_2 and the dissociation of methane hydrates from the emplacement of large igneous provinces (LIPs) have been correlated to periods of global warming and ocean anoxic events throughout geologic time (Wignall 2001). Each of these abrupt climatic events leaves a distinctive geochemical signature in the rock record which can be teased out through geochemical techniques.

Stable isotope geochemistry serves as a tool to document perturbations in the carbon cycle associated with large igneous provinces. Carbon-isotope chemostratigraphy measures the variation in $^{13}C/^{12}C$ ratios in both the organic and inorganic carbon reservoirs throughout a

stratigraphic sequence. Large variations of $\delta^{13}C$ are recorded as carbon-isotope excursions and indicate redistributions of carbon among the different carbon reservoirs (Saltzman and Thomas 2012). The emplacement of LIPs causes an influx of isotopically light carbon (^{12}C) into the oceanic and atmospheric reservoirs resulting in large negative carbon isotope excursions (NCIEs) in the rock record. NCIEs have been used as a stratigraphic tool to identify perturbations within the global carbon cycle and to correlate these perturbations amongst terrestrial and marine strata.

Stable isotope geochemistry has become a powerful tool for scientist to identify changes in geochemical cycles. Specifically, carbon isotope stratigraphy has been used to indicate fluxes in the global carbon cycle amongst the different carbon reservoirs. The goal of this research is to understand the climatic impacts to terrestrial ecosystems caused by perturbations in the global carbon cycle in western Pangea as recorded by the late Triassic to early Jurassic Whitmore Point Member (WPM) of the Moenave Formation of southwestern Utah and northern Arizona. This study uses $\delta^{13}C$ as a chemostratigraphic tool to identify perturbations within the carbon cycle during the late Triassic to early Jurassic. This time interval is characterized by abrupt climate change related to the rapid emplacement of the Central Atlantic Magmatic Province and the End-Triassic Extinction, a mass extinction event that affected both terrestrial and marine environments. I evaluated $\delta^{13}C_{organic}$ and $\delta^{13}C_{carbonate}$ at two regionally distinct stratigraphic locations within the WPM: 1) Potter Canyon, AZ and 2) Warner Valley, UT (Figure. 1). $\delta^{13}C_{organic}$ was analyzed at both locations while $\delta^{13}C_{carbonate}$ was analyzed only at the Potter Canyon locality. $\delta^{13}C_{organic}$ is analyzed from the bulk composition of terrestrial organic matter which reflects an equilibrated relationship with $\delta\ ^{13}C_{atmosphere}$. $\delta^{13}C_{carbonate}$ is analyzed from lacustrine carbonates which form in equilibrium with $\delta^{13}C$ of lake HCO_3^-. Lake HCO_3^- has an

equilibrated relationship with the $\delta^{13}C$ of atmospheric CO_2 (Deuser and Degens, 1967; Leng et al., 2004). The WPM should reflect the global carbon cycle throughout its depositional history based on $\delta^{13}C_{organic}$ and $\delta^{13}C_{carbonate}$. The use of stable isotope geochemistry will improve our understanding of terrestrial responses in both the organic and inorganic carbon reservoirs. The following objectives will be used to achieve this research goal: 1) determine if the initial negative carbon isotope excursion associated with the CAMP is present in the Moenave Formation; 2) to identify the extent of the CAMP volcanogenic effects on terrestrial organic and inorganic reservoirs and 3) to correlate global carbon isotope curves to identify the location of the end-Triassic extinction and Triassic-Jurassic boundary at various locations within the Moenave Formation.

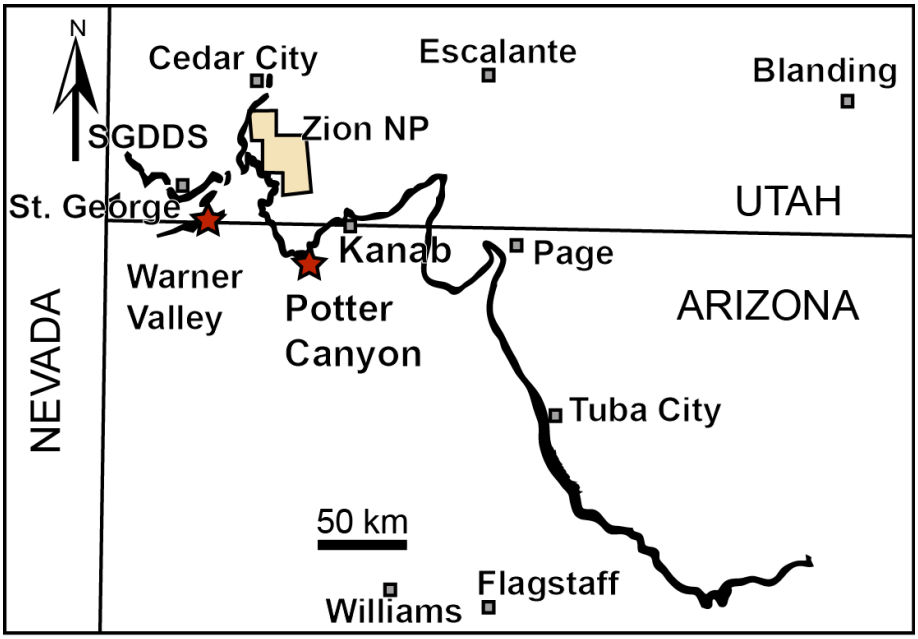

Figure 1. Sample locations (red stars) relative to the Moenave outcrop belt (thick black line). Image modified from Kirkland et al., 2014

II. BACKGROUND

A. CARBON ISOTOPE CHEMOSTRATIGRAPHY

Stable isotopes are atoms of the same element with differing amounts of neutrons within the nucleus and do not decay or emit energy. Measurement of stable isotope ratios is done via mass spectrometry. Stable isotopes are measured by the ratio of the heavy isotope to the light isotope (Eq. 1) and are reported in delta notation (δ) as per mil (‰) relative to an international standard (Eq. 2).

$$R = \frac{M_H}{M_L} \quad \text{(Eq. 1)}$$

$$\delta = \left(\frac{R_{sample} - R_{standard}}{R_{standard}}\right) \times 10^3 \quad \text{(Eq. 2)}$$

Where M_H is the mass of the heavy isotope, M_L is the mass of the light isotope, and R is the ratio between the two. Carbon and oxygen isotopes from carbonates are generally reported relative to the international standard Vienna Pee Dee Belemnite (VPDB).

Isotopic data have enormous power in determining the nature of climate change through geologic time (Marshall 1992). Organic matter ($\delta^{13}C_{organic}$) and sedimentary carbonates ($\delta^{13}C_{carbonate}$) are the main terrestrial carbon reservoirs. Both reservoirs' isotopic composition are distinctively different but are both dependent on the isotopic composition of the carbon source and the amount of carbon being redistributed amongst the different global reservoirs. The isotopic characteristics of these two reservoirs are defined by two different reaction mechanisms: 1) fractionation through isotope equilibrium exchange and 2) kinetic isotope fractionation (Hoefs 2009). Abiotic equilibrium $\delta^{13}C$ exchange reactions lead to an enrichment in $\delta^{13}C_{carbonate}$ relative to $\delta^{13}C_{atmospheric}$ (atmospheric CO_2 – dissolved bicarbonate – solid carbonate) and are independent

of temperature and crystal precipitation rate (Deuser and Degens 1968; Romanek et al., 1992). Kinetic isotope fractionation of $\delta^{13}C$ is dependent upon diffusive and biotic processes such as photosynthesis in plants, which depletes organic matter in $\delta^{13}C$ relative to $\delta^{13}C_{atmospheric}$ (Hoefs 2009). Atmospheric CO_2 is depleted in ^{13}C relative to the dissolved inorganic carbon pool. Diffusion from atmospheric CO_2 to aqueous CO_2 depletes $\delta^{13}C$ by 1.1‰ (O'Leary 1984) resulting in an isotopic composition similar to the atmosphere, whereas, HCO_3^- can be enriched by 7 – 9‰ (Degens 1967). The primary isotopic signature of organic matter and sedimentary carbonates reflect those of the isotopic signature of their environment and can be recorded in the rock record to provide vital information about carbon cycle dynamics. These dynamics are recorded in the bulk sedimentary organic and carbonate record.

Isotopic analysis of sediment to characterize carbon isotope excursions of marine and terrestrial environments has revealed changes in the global carbon cycle (Saltzmann et al., 2012). Stratigraphic variation in carbon isotope ratios may reflect changes in the carbon cycle over time that correlate to a change in bioproductivity or atmospheric greenhouse gas concentrations (Marshall 1992). This chemostratigraphic method has become a key tool in correlating global carbon cycle perturbations to events that occur within the biosphere (Saltzmann et al., 2012). Carbon isotope chemostratigraphy measures the variation in $^{13}C/^{12}C$ ratios in both the organic and inorganic carbon reservoirs throughout a stratigraphic sequence. Variations of $\delta^{13}C$ indicate redistributions of carbon among the different reservoirs within the carbon cycle. Over large time periods (millions of years) these variations are recorded as perturbations or fluctuations of exchange rates within the Earth's carbon reservoirs (Saltzmann et al., 2012).

Changes within the carbon cycle revealed by carbon isotope chemostratigraphy are termed positive and negative excursions (Figure 2). Positive carbon isotope excursions (PCIEs)

are the result of increased bioproductivity, burial of isotopically light organic matter, and a draw-down of atmospheric CO_2 (Breugel 2006). PCIEs are interpreted to be the result of oceanic anoxic events and the rapid burial of organic matter resulting in an enrichment of ^{13}C in the atmospheric and oceanic inorganic carbon reservoirs (Breugel 2006). PCIEs are typically a subsequent result of negative carbon isotope excursions (NCIEs). Negative carbon isotope excursions (NCIEs) indicate an influx of isotopically light carbon (^{12}C) into the atmospheric and oceanic carbon reservoirs. NCIEs within the rock record have been attributed to mantle degassing from the emplacement of large igneous provinces, destabilizations of methane hydrates, combustion of terrestrial organic reservoirs, and a decrease in bioproductivity (Breugel 2006, Hesselbo et al., 2002).

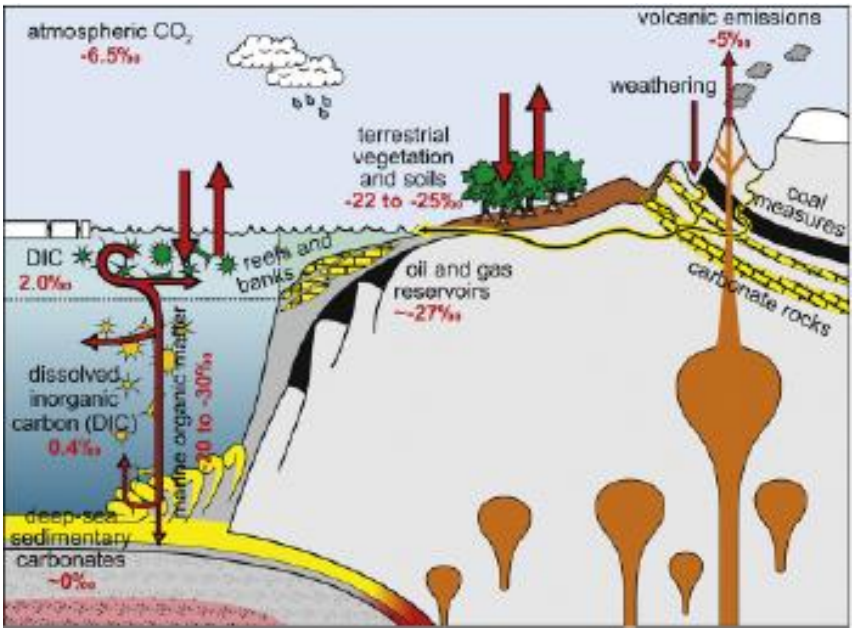

Figure 2. Global carbon cycle depicted by carbon isotope compositions of different carbon reservoirs. Image depicts pre-industrial era carbon isotope compositions. Image modified from Saltzmann et al., 2012.

B. ORGANIC AND INORGANIC CARBON ISOTOPE FRACTIONATION

Due to the relatively small size, and short residence times of the carbon reservoir, lakes respond quickly to environmental perturbations with more pronounced geochemical signals in contrast to oceans, which have longer residence times for carbon. (Hollander and McKenzie 1991). Organic matter and carbonates are the principle carbon sinks in a lacustrine environment. Carbon isotopes are fractionated as they transition through the carbon cycle in both the organic and inorganic carbon pools (Leng et al., 2004). Fractionation mechanisms are different for both pools and are contingent upon biotic and abiotic kinetic and equilibrium processes. Lakes produce primary mineral precipitates in the form of authigenic and biogenic carbonates. Authigenic carbonates are generally precipitated in the form of minerals such as calcite and aragonite or as a response to algal and macrophyte photosynthesis (Leng et al., 2005). Biogenic carbonates (shells) are precipitated from organisms such as ostracods and mollusks (Leng et al., 2005). $\delta^{13}C$-values from biogenic carbonates can vary erratically due to local habitat effects, incorporation of metabolic carbon, and speciation (Talbot 1990). Bulk $\delta^{13}C_{carbonate}$ analyzes both authigenic and biogenic carbonates, which can cause some discrepancies because various carbonate mineral precipitates have different mineral-water isotope fractionation effects (Leng et al., 2005); however, lacustrine authigenic and biogenic carbonates are dependent upon atmospheric carbon ($\delta^{13}C_{atmosphere}$) and should respond according to atmospheric changes. $\delta^{13}C_{carbonate}$ is also primarily dependent on the temperature, pH, and isotope composition of the lake waters from which they precipitate (Leng et al., 2005).

Organic matter also provides carbon for isotopic analysis. Organic matter preserved within lacustrine settings generally consists of lipids, carbohydrates, proteins and plant organic matter from in and around the lake (Leng et al., 2005). Organic matter in a lacustrine

environment is both allochthonous and autochthonous. Autochthonous organic matter generally consists of terrestrial C_3 photosynthesizing plant materials, aquatic plants (macrophytes) and phytoplankton while allochthonous organic matter can be recycled from underlying and sometimes much older lithologic units. Photosynthesizing organisms obtain carbon from one of three sources: 1) atmospheric CO_2, 2) aqueous CO_2, and 3) dissolved inorganic carbon (DIC, i.e. HCO_3^-). An organism's isotopic composition will be influenced by the $\delta\,^{13}C$ of the carbon source used during photosynthesis (Degens 1967). Carbon isotope fractionation in organic matter is controlled by pH, water temperature, concentration of carbonic acid species, and by metabolic effects and growth rates of the organism (Degens 1967). Maximum fractionation occurs when dissolved CO_2 concentrations are high, growth rates are moderate, and water pH and temperature are low (Degens 1967). However, metabolic effects such as photosynthesis are principal controls of carbon isotope fractionation in organic matter. Overall, carbon fixed through photosynthesis can be depicted by the following equation:

$$CO_2 + H_2O \rightarrow CH_2O + O_2$$

C_3 photosynthesis has been the dominant photosynthetic pathway through geologic time. Plants using the C_3 pathway generally have a $\delta^{13}C$ that is approximately 20‰ less than the $\delta^{13}C$ of the atmosphere. This discrimination of ^{13}C during C_3 photosynthesis is the result of a multistep process consisting of two main phases of discrimination: 1) gaseous diffusion through the boundary layer and stomata of the leaf, and 2) by the carboxylating enzyme, ribulose-1, 5-biphosphate (RuP_2) carboxylase (Park and Epstein 1960; Farquhar et al., 1982). Fractionation, first starts with CO_2 diffusing through the boundary layer and the stomata of the leaf. Diffusivity of $^{12}CO_2$ through air is 4.4‰ greater than the diffusivity of $^{13}CO_2$; therefore, an open stomata will discriminate against $\delta^{13}C$ by -4.4‰ (Craig 1953; Farquhar et al., 1982; Schlesinger and

Bernhardt 2013). A greater portion of $^{12}CO_2$ will enter the leaf than $^{13}CO_2$ over any period of time, and if CO_2 is not a limiting factor the preference for ^{12}C will be greater, thus lowering the $\delta^{13}C$ (Schlesinger and Bernhardt 2013). The next step of ^{13}C discrimination is controlled by the carboxylating enzyme, ribulose-1, 5-biphosphate (RuP_2) carboxylase (Rubisco) (Park and Epstein 1960; Farquhar et al., 1982). This metabolic process ultimately controls the overall $\delta^{13}C$ composition of the plant, in that the fractionation in the overall reaction is ~-20‰; however, other components such as carbohydrates and amino acids also show different degrees of ^{13}C fractionation relative to atmospheric or dissolved CO_2 (Degens 1967). Lipids also tend to be depleted in ^{13}C relative to bulk plant organic matter (Figure 3). C_3 photosynthesis is also observed within aquatic plants; however, the ability for an aquatic plant to preferentially fixate carbon from the dominating carbon species will affect its overall carbon isotope composition.

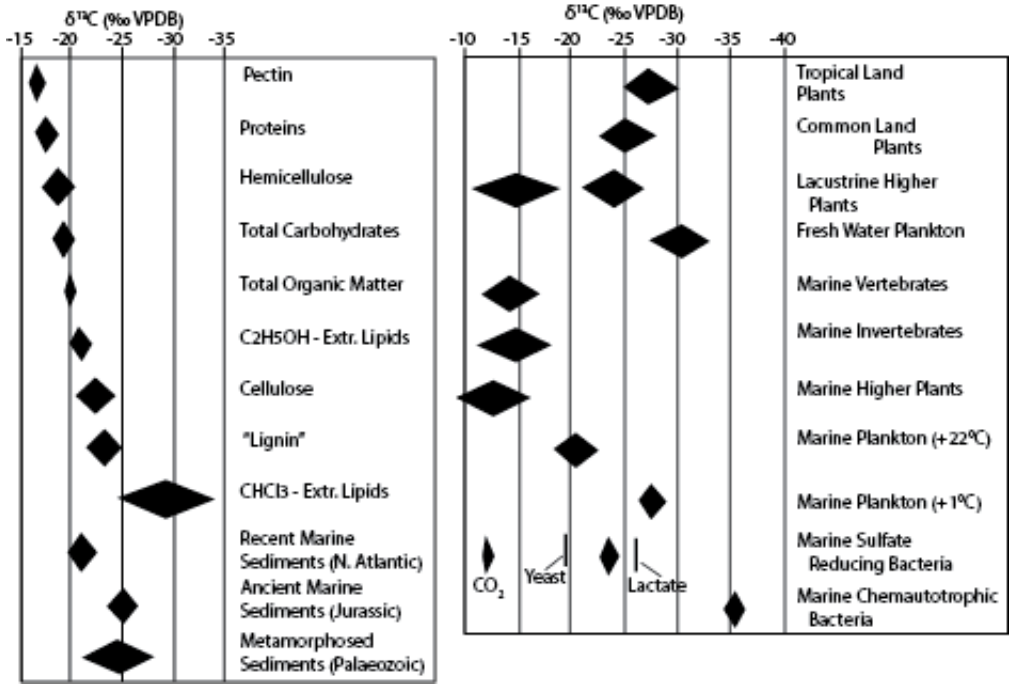

Figure 3. Left: Carbon isotope compositions for various organic compounds. Right: Carbon isotope compositions for different organisms. Diamond represents the $\delta^{13}C$ range for each reservoir. Center of the diamond indicates the average $\delta^{13}C$ for each reservoir. Note that

lacustrine higher plants can have two distinctive $\delta^{13}C$ based on the dominating carbon specie in the system. Image modified from Degens 1967.

Two carbon fixating behaviors can be observed in lacustrine plants causing different plants to fractionate based on the environments dominant carbon species. This is generally dependent on environmental conditions and ultimately affects aquatic plants' isotopic composition (Figure 3). Aqueous photosynthesis can utilize $CO_{2(aq)}$ or HCO_3^- depending on which one is the dominant carbon species. The dominant carbon species is dependent upon the pH of the environment (Figure 3). Diffusion of CO_2 through water in aquatic photosynthesis is 10^4 times slower than through air and is a limiting factor for photosynthesis (Pederson et al., 2013). This is a major control on the isotopic composition of aquatic plants and leads to a decrease in carbon isotope fractionation amongst aquatic plants, even C_3 plants (O'Leary 1988) causing aquatic plants to be enriched relative to terrestrial C_3 plants. CO_2 diffusion through an aqueous solution results in a decrease in $\delta^{13}C$ by 0.7‰ (O'Leary 1984). HCO_3^- is the dominant carbon species in aquatic environments with a pH range of ~7-10 (Leng et al., 2004). Aquatic plants, unicellular algae and macroalgae can utilize HCO_3^- for photosynthesis during an increase in pH or when $CO_{2(aq)}$ is limited (< 10 μmol/l) (Hollander and McKenzie, 1991; Pederson et al., 2013). Aquatic plants can use HCO_3^- via two different ways during aqueous photosynthesis: 1) direct uptake through cells or 2) external conversion of HCO_3^- to $CO_{2(aq)}$ in the diffusion boundary layer. The isotopic fractionation between $CO_{2(aq)}$ and HCO_3^- is generally +9‰ but can range in enrichment between 12.0‰ to 8.4‰ in temperatures varying 0 to 30°C (Deuser and Degens 1968, O'Leary 1988, Romanek 1991) and plants that utilize it as a source for carbon will display heavier $\delta^{13}C$ values than C_3 aquatic plants using $CO_{2(aq)}$.

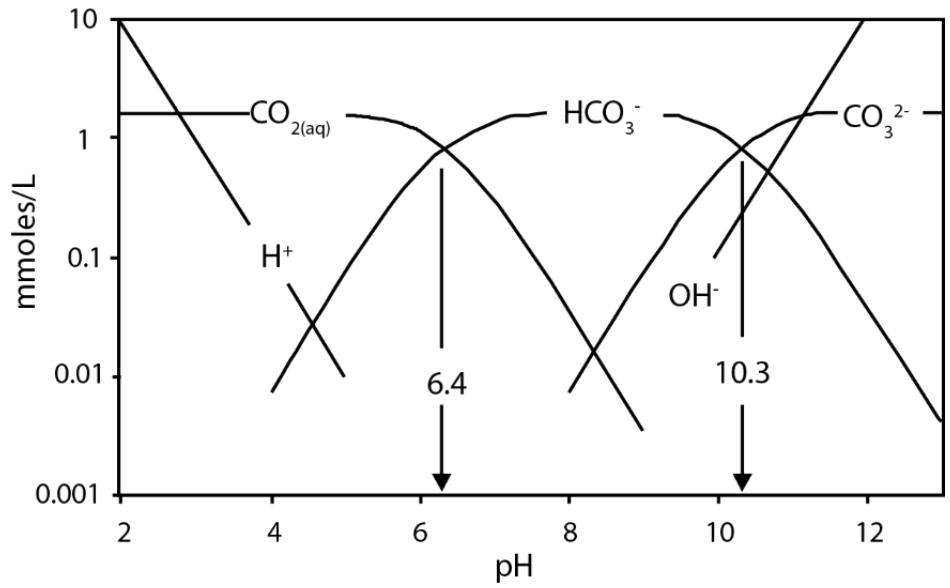

Figure 4. Bjerrum plot showing the distribution of carbon species in water as a function of pH at 25°C.

Phytoplankton are an important source of organic matter in lacustrine environments. Sediment traps in lakes have shown that 1-35% of organic matter from the photic zone reaches the sediment surface (Lehmann et al., 2002 and references within). Phytoplankton are depleted in ^{13}C relative to inorganic carbon sources due to the fractionation process and the preferential use of $CO_{2(aq)}$ during photosynthesis (Burkhardt et al., 1999) resulting in a $\delta^{13}C$ range of -42 to -26‰ (Leng et al., 2004). The carbon isotopic composition of phytoplankton is largely controlled by intracellular and extracellular CO_2 concentrations, phytoplankton growth rate and cell geometry, light intensity, water temperature and pH, and the use of $CO_{2(aq)}$ vs. HCO_3^- (Burkhardt et al., 1999; Degens 1967; Deuser et al., 1967; Popp et al., 1997; Popp et al., 1998).

Authigenic and biogenic carbonates incorporate inorganic carbon isotopes from TDIC (total dissolved inorganic carbon) in lacustrine settings through equilibrium and kinetic fractionation processes (Leng et al., 2005); however, kinetic fractionation is often minor and is often independent of temperature and crystal growth rate (Romanek et al., 1992). The $\delta^{13}C$ of

TDIC is controlled by the dominating carbon supply source to the lacustrine environment. Three processes control the isotopic composition of $\delta^{13}C_{TDIC}$: 1) the isotopic composition of inflowing waters, 2) CO_2 exchange between atmosphere and lake water, and 3) photosynthesis/respiration of aquatic plants (Figure 5) (Leng et al., 2004). Precipitated calcite from ground and river waters have low $\delta^{13}C_{TDIC}$ values between -10‰ and -15‰ (Leng et al., 2004). Decaying organic matter at the sediment–water interface liberates isotopically light CO_2 with isotopic compositions between -32‰ and -27‰. In waters with a pH ranging between 7- 10, HCO_3^- becomes the dominant carbon species (Figure 4) and is enriched by 9 to 10‰ compared to CO_2 (Degens 1967, Romanek et al., 1992, Leng et al., 2004). If inflowing waters (surface and ground) are the dominating carbon source and isotopic controls then $\delta^{13}C_{TDIC}$ will be depleted relative to atmospheric CO_2. An increase in pH and salinity will control the dominant carbon species during dry and evaporative lake conditions (Leng et al., 2005). This reduces the concentration of $CO_{2(aq)}$ and increases the concentrations of HCO_3^- which is enriched by ~9‰ relative to atmospheric CO_2. This would primarily be a function in open lake systems. Closed lakes precipitate carbonates that are in isotopic equilibrium with atmospheric CO_2. If atmospheric CO_2 is the controlling factor on $\delta^{13}C_{TDIC}$ then the $\delta^{13}C_{TDIC}$ will be enriched by ~9 to 10‰ relative to atmospheric CO_2. Photosynthesis/respiration can influence $\delta^{13}C_{TDIC}$ in a lake during periods of increased productivity and can be a product of seasonality (Leng et al.,2004). Preferential uptake of ^{12}C by photosynthesizing organisms will enrich the TDIC pool. Due to their ability to record environmental perturbations, lacustrine carbonates are a strong tool for tracing changes in the carbon cycle at a localized and global level.

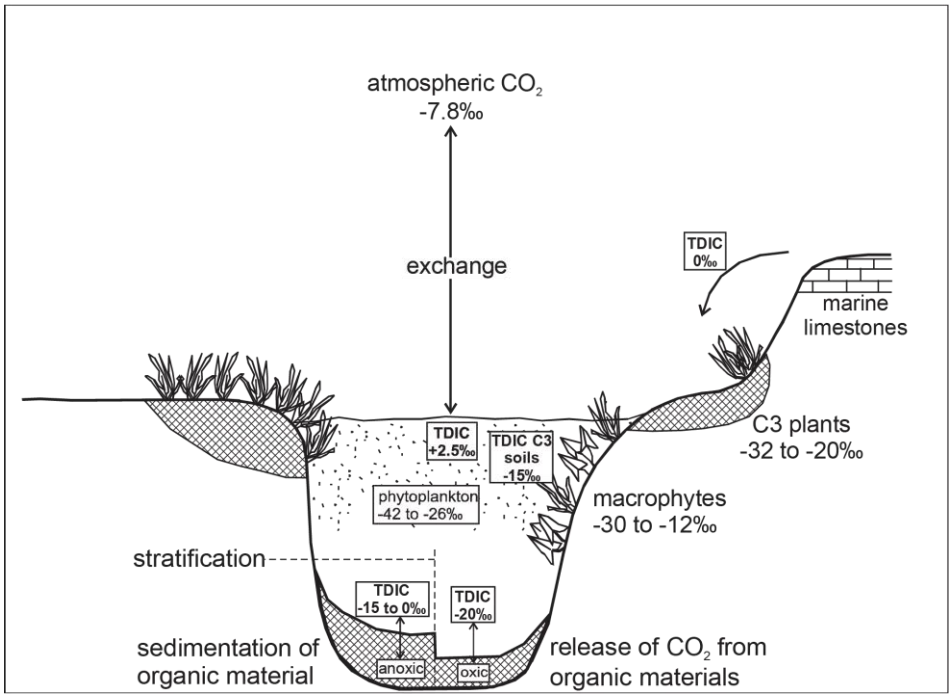

Figure 5. Carbon isotope values for the major sources of carbon in a lacustrine environment and examples of the range of $\delta^{13}C_{TDIC}$ as a result of the dominant source. C_4 plants and $\delta^{13}C_{TDIC}$ reflecting C_4 have been removed because of the absence of C_4 plants during the Triassic and Jurassic. Image modified from Leng et al., 2004.

C. EFFECTS OF DIAGENESIS ON CARBON ISOTOPES

Syn-depositional and post-depositional diagenesis can affect the overall isotopic composition of sediment through time, distorting past geologic climate records. Diagenesis is defined as syn/post depositional chemical change that can affect sediment or minerals (Marshall 1992). The potential of alteration to the primary isotopic signal of sedimentary organic matter and carbonates needs to be properly assessed in order to reconstruct past environmental changes. Both sedimentary organic matter and carbonates are susceptible to diagenesis by a variety of changing environmental preservation factors.

Understanding the isotopic effects of diagenesis during organic-matter decomposition will determine the viability of stable isotope ratios from organic matter to be used as indicators for past environmental perturbations (Lehman et al., 2002). Oxic and anoxic conditions degrade

and preserve matter differently. Organic-matter decomposition is primarily mediated by aerobic and anaerobic microbial processes (Lehmann et al., 2002). Reactive organic compounds will degrade in oxic and anoxic conditions at similar rates; however, the proportion of organic matter resistant to degradation is much higher under anoxic conditions (Lehmann et al., 2002). Early stages of diagenesis in organic matter will tend to preferentially eliminate ^{13}C-rich compounds such as proteins or carbohydrates (Degens 1967). Decarboxylation of a ^{13}C enriched molecule will cause a decrease in its remaining $\delta^{13}C$ ratio while releasing CO_2 enriched in $\delta^{13}C$ (Degens 1967). Carbohydrates and proteins are typically enriched in $\delta^{13}C$ relative to lipids and are more susceptible to microbial degradation which leads to a depleted pool of residual organic matter in sediments (Harvey et al., 1995; Lehmann et al., 2002). Carbohydrates are utilized most rapidly under oxic conditions, followed by proteins and then lipids. Lipids are usually the most highly preserved biochemical class because of the tendency for carbohydrates and proteins to decay more rapidly (Harvey et al., 1995). Oxic conditions tend to degrade organic material while anoxic conditions enhance preservation (Lehmann et al., 2002). Experimental and field studies have shown that oxic and anoxic degradation of organic matter will decrease the $\delta^{13}C$ of organic matter by about 1.5 – 1.6‰ (Lehmann et al., 2002). Overall, the main processes that affect the preservation and $\delta^{13}C$ of organic matter are isotope fractionation during decomposition of organic compounds, selective preservation of isotopically distinct organic matter, and bacterial photosynthesis (Lehmann et al., 2002).

Carbonate cementation and replacement during post-depositional diagenesis can obscure primary isotopic signals (Marshall 1992). Carbon isotopes in carbonates are less prone to alteration during diagenesis than oxygen isotopes but shifts can occur when organogenic carbon is incorporated (Figure 5) (Marshall 1992). Cross plotting $\delta^{13}C$ and $\delta^{18}O$ alone as a geochemical

approach to assessing diagenesis in carbonates is an insufficient technique, especially if plotting bulk carbonate. Petrographic, stratigraphic, and geochemical data must be combined and analyzed to fully demonstrate the effects of diagenesis through water-rock interaction (Lohmann 1988). Cathodoluminescence along with petrography can identify diagenetic $CaCO_3$. Diagenetic $CaCO_3$ tends to be highly luminescent when compared to primary $CaCO_3$. The diagenetic potential of carbonates depends on the solubility of the mineral components. Low-Mg calcite is less soluble and less reactive compared to aragonite and high-Mg calcite (Marshall 1992). This implies that aragonite and high-Mg calcite are more susceptible to diagenesis than low-Mg calcite. Terrestrial carbonate diagenesis is typically the result of recrystallization and replacement of carbonate constituents through water-rock interaction. Diagenesis of terrestrial carbonates through water-rock interaction should affect oxygen isotopes more than carbon isotopes unless the isotopic composition of the water is enriched or depleted in $\delta^{13}C_{DIC}$ or there is an effect by organogenic carbon (Marshall 1992).

D. CENTRAL ATLANTIC MAGMATIC PROVINCE

The rifting of Pangea during the late Triassic to early Jurassic (~200 MYA) has been associated with the emplacement of voluminous amounts of dikes, sills and lava flows known as the Central Atlantic Magmatic Province (CAMP) (Marzoli et al. 1999). Currently, these dikes, sills and lava flows are preserved in circum-Atlantic Triassic basins in the United States, Morocco and South America (Beutel et al. 2005 and references within). The Central Atlantic Magmatic Province is a combination of two large igneous province (LIPs) types: 1) continental flood basalts and 2) volcanic rifted margins (McHone 2003, Bryan et al. 2007). The CAMP is one of the most voluminous and aerially extensive LIPs emplaced during the Phanerozoic with an estimated volume of 3-11 x 10^6 km^3 and an estimated area greater than 2.5 x 10^6 km^2 (Fig. 6)

(Marzoli 1999, McHone 2003, Blackburn et al 2013). Geochronological age measurements (Ar-Ar, and U/Pb) have constrained the rifting and emplacement of the CAMP to take place between 202 – 190 Ma with the main magmatic peak of the CAMP occurring between 201.5 and 200.0 Ma (Nomade et al. 2007, Schoene et al. 2010, Marzoli et al. 2011, Blackburn et al. 2013) The CAMP's magmatic peak was short in duration, lasting approximately 1.6-2 m.y with much of its extrusive activity lasting << 1 Ma (Marzoli et al. 1999, Nomade et al. 2007).

Figure 6. Paleogeography of Earth at ~200 Ma. Red shading is the estimated global extent of the Central Atlantic Magmatic Province (CAMP) simplied from McHone 2003. Red dots indicate previously researched locations: 1) St. Audrie's Bay, UK (Hesselbo et al., 2002); 2) and 3) Newark and Hartford Basins (Whiteside et al., 2010); 4) Astartekloft, Greenland (Hesselbo et al., 2002); 5) Kuhjoch, Austria (Ruhl et al., 2009); 6) New York Canyon, NV (Guex et al., 2004); and 7) Kennecott Point, BC (Ward et al., 2001) Yellow dot indicates approximate location for the current study area. C is the estimated plume center for the CAMP. Image modified from Ruiz-Martinez et al., 2012.

Climatic impacts of the CAMP have been extensively modelled and identified within the rock record. Estimates of the volatile emissions from the CAMP indicate enough volatiles were degassed to induce a global environmental catastrophe. Volatile gas emissions (SO_2, CO_2 and halogens) from the CAMP are estimated to be between 1.11×10^{12} and 5.19×10^{12} metric tons (McHone 2003). Carbon emissions released as CO_2 and CH_4 during the emplacement of the CAMP are estimated to be ~8,000-9,000 and ~5,000 gigatons respectively (Beerling and Berner 2002). Empirical data obtained from the leaf stomata ratios and pedogenic carbonates have been used to estimate atmospheric CO_2 concentrations. McElwain et al. 1999 used leaf stomata ratios from fossilized Ginkgoalean and Cycadalean leaves to estimate a change in atmospheric CO_2 concentration from 600 ppm to 2100-2400 ppm across the Triassic – Jurassic boundary. Pedogenic carbonates from the Newark and Hartford basins estimate a change in atmospheric CO_2 concentrations from the pre-eruptive background concentration of 2,000 ppm to ~4,500-5,000 ppm (Schaller et al., 2011, 2012, and 2014). Mean global temperature changes associated with this abrupt rise in atmospheric CO_2 have been estimated to be 3°- 4°C, with models estimating a potential 6°C increase (McElwain et al. 1999, Huynh et al. 2004). A mean global temperature change of 3° to 6°C would have driven selection amongst terrestrial vegetation to avoid lethal leaf limits aiding in the >95% turnover in megafloral species during the end Triassic extinction (McElwain et al. 1999).

An increase in the atmospheric CO_2 concentrations of this magnitude and a release of methane from buried methane hydrates would cause major perturbations to the global carbon cycle. Several $\delta^{13}C_{carbonate}$ and $\delta^{13}C_{organic}$ chemostratigraphic records of the late Triassic to early Jurassic show an initial negative carbon isotope excursion (NCIE) associated with the CAMP (Figure 7) (Ward et al., 2001; Palfy et al., 2001; Hesselbo et al., 2002; Guex et al., 2004; Galli et

al., 2005; Williford et al., 2007; Whiteside et al., 2010; Ruhl et al., 2009; Bacon et al., 2011). This initial NCIE has been reported in both marine and terrestrial environments and has a magnitude of varying between -3.5‰ to -8‰ (Palfy et al., 2001; Ruhl et al., 2009). An excursion of this magnitude represents a major carbon cycle perturbation through volcanic activity and methane release. Thus, carbon isotope chemostratigraphy can be used as a marker for identifying the increased CO_2 concentrations associated with the CAMP.

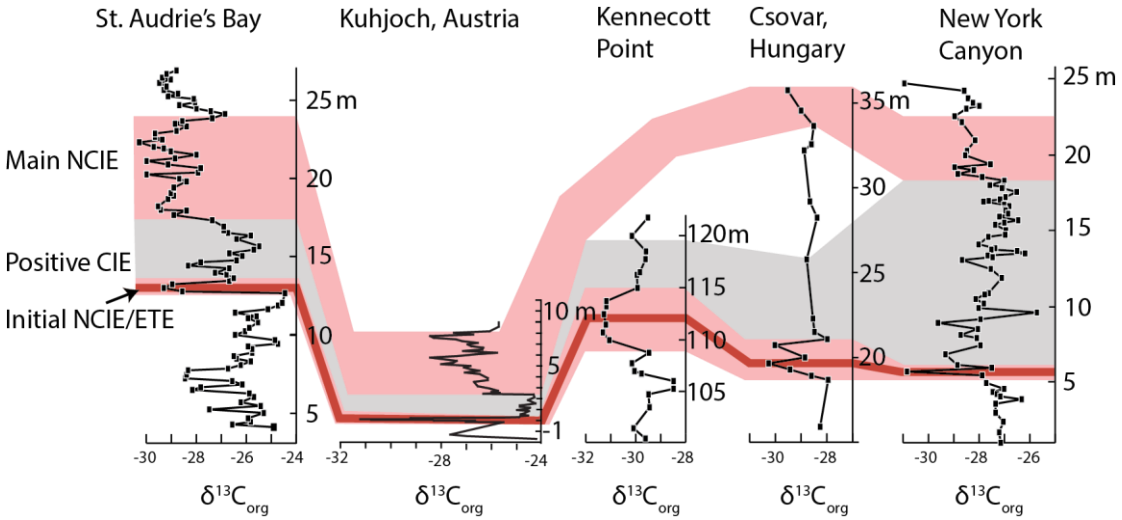

Figure 7. Late Triassic to early Jurassic global carbon isotope stratigraphy trends from previous studies in both marine and terrestrial strata. Most sections are characterized by an initial negative carbon isotope excursion (NCIE) that is associated with the end-Triassic extinction, followed by a positive shift and a main drawn out NCIE. St. Audrie's Bay (Hesselbo et al., 2002); Kuhjoch, Austria (Ruhlet al., 2009); Kennecott Point (Ward et al., 2001); Csovar, Hungary (Palfy et al., 2001); New York Canyon (Guex et al., 2004)

E. END-TRIASSIC EXTINCTION

The end-Triassic extinction (ETE) is the third largest mass extinction of the Phanerozoic era affecting both terrestrial and marine biota (Raup and Sepkoski 1984). The ETE is characterized by a 30% loss of marine genera, 50% loss of tetrapod species, and a 95% turnover of megafloral species (McElwain et al. 1999). Blackburn et al., (2013) dated the ETE to have

occurred between 201.564 ± 0.015/0.22 MYA. The ETE occurs synchronously with early phases of the emplacement of the CAMP indicating a cause and effect relationship between the two events (Figure 8) (Blackburn et al., 2013) and lasted ~20-40 kya (Ruhl et al., 2009).

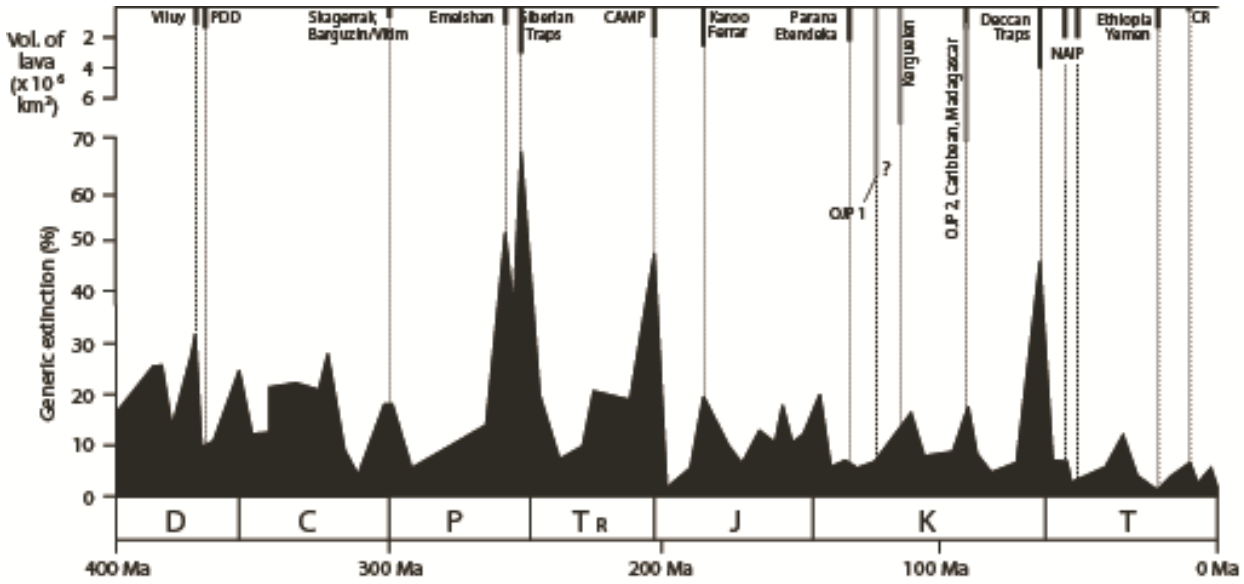

Figure 8. Correlation of extinction events with the emplacement of large igneous provinces (LIPs) over the past 400 Ma. Light shaded LIPs indicate oceanic plateau basalts and dark color LIPs represent continental flood basalts. Note the relationship between continental flood basalts and generic extinction (%). Image modified from Bond and Wignall 2014.

In the marine realm, elevated CO_2 resulted in a temporary under saturation of sea water with respect to aragonite and calcite and may have caused a decrease in carbonate sedimentation and a reduction in primary productivity (McRoberts and Newton, 1995; Hautmann 2004). Fossil evidence shows a replacement of aragonite by calcite in marine biota as an evolutionary response to elevated atmospheric CO_2 levels. As a result, aragonitic and high magnesium calcite secreting organisms would have suffered high extinction rates (Hautmann 2004). Reef production decreased as a result of $CaCO_3$ under saturation leading to extinction of major aragonite secreting reef organisms such as: spongiomorphs, inozoid and sphictozoid sponges, tabulozoans, disjectoporids, scleractinian corals and involutinid foraminifers (Hautmann 2004 and references

within). Aragonite shelled mollusks had the highest extinction level while only six superfamilies and one genus (*Psiloceras)* of ammonids survived the ETE (Hallam and Wignall 1997, Hautmann 2004). A decrease in primary productivity lead to a greater survivorship of epifaunal bivalves *versus* infaunal bivalves (Hautmann 2004). Conodonts became completely extinct and almost all Sauropterygian marine reptiles that dominated the seas became extinct with the exception of plesiosauri ancestors.

The effects of the CAMP had the strongest consequences for terrestrial genera, specifically on floral species. The "fern-spike' observed in late Triassic to Jurassic strata is indicated by a spike in the abundance of fern spores that occur in the strata encompassing the ETE and the initial NCIE (McElwain et al., 1999; van de Schootbrugge et al., 2009; Bonis and Kürschner 2012). A sharp transition from a diverse pollen assemblage of bisaccate and monosaccate pollen to 60-90% monospecific assemblage of the pollen *Classopollis meyeriana* occurs between strata directly below the first Newark Basin flood basalts to the strata directly overlying the flood basalts (Fowell and Olsen 1995). A >95% turnover in megafloral species is coupled by a significant decrease in leaf size and leaf dissection that are associated with increases in CO_2 and temperature (McElwain et al. 1999). McElwain et al., (1999) showed that a 3-4°C global mean temperature change would have caused significant thermal damage to broad-leafed taxa therefore causing selection amongst flora to avoid lethal leaf temperatures. For example, there is an observed reduction in the number of broad-leaf taxa in the canopy such as *Ginkgoites obovatus* leading to the replacement by dissected leaf taxa such as *Ginkgoites fimbriatus* (McElwain et al., 1999). Species that do not show a decrease in abundance were genera with dissected leaves or narrow leaves such as *Clathopteris meniscoides* and *Equisetites muensteri* (McElwain et al., 1999). Regional climate and environmental change related to the

emplacement of the CAMP resulted in a loss of plant biodiversity and non-uniform, climate dependent, vegetation change (McElwain et al., 2009; Bonis and Kurschner, 2012). The greater than 95% extinction to megafloral species caused a significant habitat and food crisis for tetrapod fauna. By the end of the Triassic the herbivorous aetosaurs and their dominant predators, phytosaurs became extinct allowing for the continued radiation of dinosaurs into the Jurassic.

F. TRIASSIC – JURASSIC BOUNDARY

There is a distinctive difference between the end Triassic Extinction and the Triassic – Jurassic boundary. The Global Boundary Stratotype Section and Points (GSSP) defines the Triassic-Jurassic boundary not as an interval of extinctions but rather as the first occurrence of *Psiloceras spelae tirolicum,* a European subspecies of ammonite at the Kuhjoch section in Austria (Milner et al., 2012). The Triassic – Jurassic marine boundary has been dated to be 201.31± 0.18/0.38/0.43 (Schoene et al., 2010). This date was obtained from $^{206}Pb/^{238}U$ of zircons contained in ash beds in the Pucara Basin of Peru that occur contemporaneously with *P. spelae*. An issue that arises when defining a boundary based off marine ammonite subspecies is correlating the boundary to terrestrial strata. Kozur and Weems (2010) proposed the importance of using conchostracans as a terrestrial biostratigraphic indicator. Conchostracans are widespread in fluvial, lacustrine and flood deposits and can have a high stratigraphic resolution comparable to that of ammonites (Kozur and Weems 2010). Kozur and Weems (2010) established a conchostracan zonation from the late Permian (Changhsingian) to the early Jurassic (Hettangian). This zonation suggests that conchostracans can be used as biostratigraphic indicators within terrestrial strata. Conchostracan biostratigraphy can be correlated to marine substages of the Triassic and are constrained by interbedded ostracod zones, palynology zones, distinctive facies shifts, and cycle-scaled mangetic magnetozones (Kozur and Weems, 2010; Ogg 2012). The

Triassic-Jurassic boundary is characterized as a transition from *Euestheria brodieana* (Rhaetian) to *Bulbilimnadia killianorum* (Hettangian) (Kozur and Weems, 2010; Lucas et al., 2011).

Ichnotaxa are commonly used, especially in the Newark Basin, as a biostratigraphic indicator. Crurotarsan-type tracks (archosaurs) such as *Brachychirotherium* give way to dinosaurian track such as *Eubrontes* (Lucas and Tanner, 2007; Tanner and Lucas 2009, Ogg 2012). Crurotarsan tracks are not found in the Jurassic, while in the Newark basin, *Eubrontes* is found only in Jurassic strata.

G. MOENAVE FORMATION

1. STRATIGRAPHY

The late Triassic (Rhaetian) to early Jurassic (Hettangian) Moenave Formation of southern Utah and northern Arizona consists of fluvial and lacustrine depositional environments occurring in a retro-arc basin that formed on the western edge of the North American craton as a result of collision with the Cordilleran magmatic arc system (Tanner and Lucas, 2009). The Moenave Formation (Figure 9) consists of two primary lithostratigraphic members: 1) the Dinosaur Canyon Member (DCM) and 2) the Whitmore Point Member (WPM) (Tanner and Lucas, 2009; Milner et al., 2012; Kirkland et al., 2014). The basal contact of the Moenave Formation is with the underlying Chinle Formation (Late Triassic). This is an abrupt erosive contact in which the basal conglomerate erodes the top of the Owl Creek Member of the Chinle Formation with up to 20cm relief on the erosive surface. The Kayenta Formation lithostratigraphically overlies the Moenave Formation and is defined by the J –0’ unconformity between the Springdale Sandstone of Kayenta and the Whitmore Point of the Moenave. The Wingate Sandstone is chronostratigraphically related to the Moenave Formation and is representative of an erg. The

Kayenta Formation and Wingate Sandstone inter-finger with the Moenave Formation to the northeast of the Moenave outcrop belt.

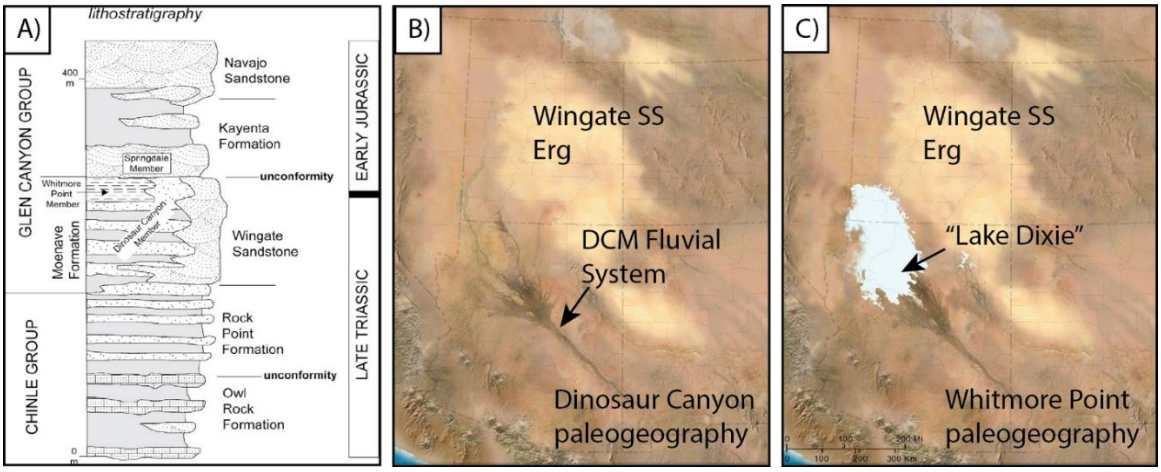

Figure 9. A) Stratigraphic section of the Moenave Formation from Lucas et al., 2011. B) Paleogeographic map showing the depositional environment of the Dinosaur Canyon fluvial system. C) Paleogeographic map showing the depositional environment of the Whitmore Point Member. Paleogeographic map depicts the maximum extent of the ephemeral "Lake Dixie." Paleogeographic maps courtesy of Ron Blakey, modified from Milner et al., 2012.

2. LITHOLOGY

The Mogollon Highlands and initial uplift of the Colorado Plateau provide the source sediment for the Moenave Formation. Typical sedimentological trends for the Moenave formation show an increase in grain size towards the east and an increase in mud/clay content towards the west suggesting an eastern provenance (Davis 1977). The Dinosaur Canyon Member (DCM) is composed of conglomerates, sandstones, siltstones and mudstones and relative to the WPM is more sand-dominated. These sequences represent a northwest trending alluvial system of fluvial, overbank, and lacustrine deposits. The lower part of the DCM is dominated by reddish-brown fine-grained sandstone with occasional ripple-bedded units and mud cracked surfaces. The upper part of the DCM is dominated by a cliff-and ledge forming pale reddish-brown sandstone and mudstone. Sedimentary structures include medium-scale trough cross-

bedded sandstones that grade to tabular bedding and ripple drift laminae. The upper-most DCM also contains abundant plants that include fragments of ferns, horsetails, and conifer remains such as *Araucarites*, *Saintgeorgia*, and *Milnerities* (Tidwell and Ash, 2006). In fine-sand units of the upper DCM, abundant tracks are found such as dinosaurian tracks of *Grallator* and *Eubrontes* and the crocodylomorph *Batrachopus*. The uppermost DCM represents aggradational river channel deposits with increasing shallow wave-dominated lacustrine shoreline deposits as the ancient "Lake Dixie" formed.

In other localities the Whitmore Point-Dinosaur Canyon Member is marked by the change from fluvial dominated clay-rich sandstones to ripple cross-laminated shaley mudstones and fine sandstones. Kirkland et al., (2014) suggests that the boundary between the two should be represented by the transition from fluvial dominated sandstones and mudstones to lacustrine dominated shore-line sandstones or distal lacustrine shales.

The Whitmore Point Member represents a shallow perennial lacustrine environment along the north to northwest trending Dinosaur Canyon alluvial system as evident by small stromatolitic mounds, salt and gypsum casts, and abundant mud cracks. The terminal floodplain and occasional flood outs of the Dinosaur Canyon fluvial system provided clastic sediments which comprise the Whitmore Point. The Whitmore Point Member has variable stratigraphic thicknesses along the Moenave outcrop belt but overall has been divided into three distinctive lithologic intervals: 1) a lower shale and sandstone interval, 2) a middle sandstone dominated interval and 3) an upper shale dominated interval (Fig. 10). The entire Whitmore Point represents two lake megacycles, a thick lower cycle and a thin upper cycle (bounded by the middle proximal sandstone) that are the remains of an ancient lake termed "Lake Dixie"(Milner et al., 2012).

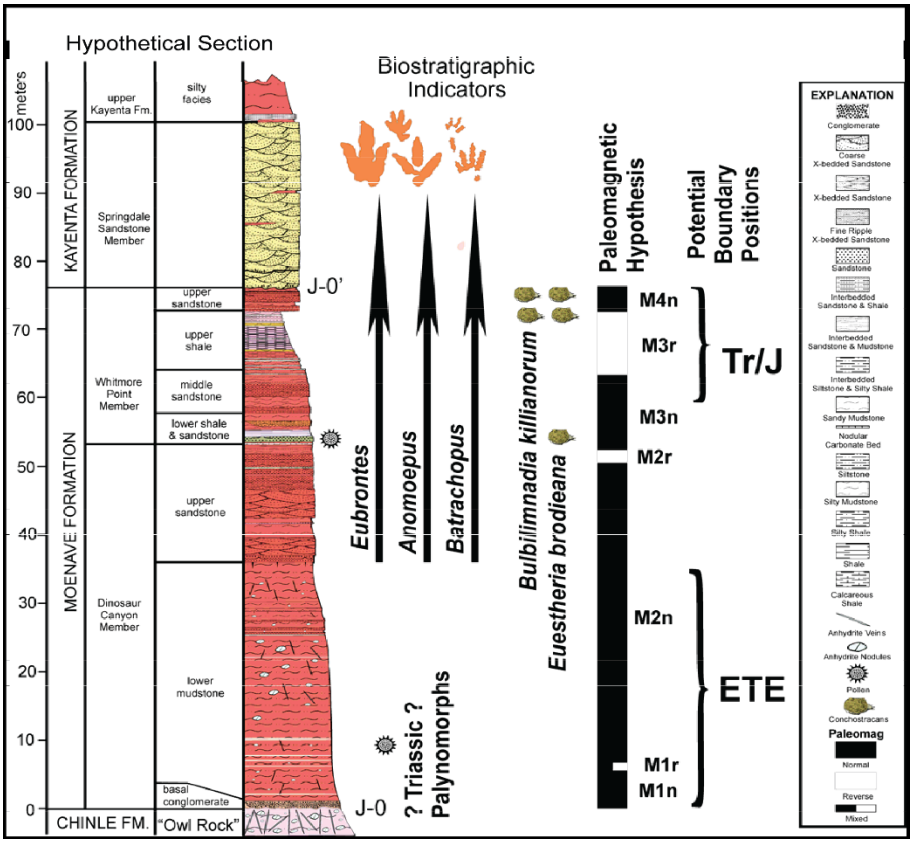

Figure 10. Hypothetical stratigraphic section of the Whitmore Point Member showing lithologic packages, biotstratigraphy, magnetostratigraphy and potential Triassic – Jurassic and end-Triassic extinction boundaries. Note that the Whitmore Point and Dinosaur Canyon Members have a diachronous relationship. Paleomagnetic data is modified from Donohoo-Hurley et al., 2010. Image is modified from Kirkland et al., 2014.

The lower shale and sandstone interval of the WPM has been divided into two separate packages: 1) a lower shale unit and 2) an upper sandstone unit. The lower unit has been described as a well-laminated, poorly to moderately indurated dark organic and calcareous shale unit. This interval is highly fossiliferous containing well-preserved ostracodes, conchostracans; a thin stromatolite layer; and plant fragments and fish debris. The upper sandstone dominated unit consists of a grayish-red silty shale with a thin sandstone layer on top, both of which are unfossiliferous. Lenticular sandstone beds are exhibited at some outcrops of the WPM in this lower sequence. These lenses are meters thick and not laterally extensive. They display large-

scale soft-sediment deformation features such as over-steepened rotated bedding, minor folding, and water escape structures. Laminar and trough-cross-bedding occur where the sandstone lenses are not deformed. This lower sequence of the WPM is interpreted as a distal lacustrine environment that was partially in the photic zone of the lake, allowing the formation of stromatolites. The sandstone lenses in the upper part of this interval are interpreted as channels that formed during periods of reduced depositional base level (Kirkland et al., 2014).

The middle sandstone interval overlies the lower shale and sandstone interval. This interval is dominated by fine to medium grained sandstone beds with interspersed sandy mudstone intervals. Sandstone layers display ripple cross-bedding, mudcracks, burrows and the dinosaur cracks *Grallator* and *Anomepus*. This interval is dominantly a cliff forming unit of the WPM. This middle sandstone interval is interpreted as a migrated sandbar or spit.

The upmost interval of the WPM is the upper shale interval. This interval is described as being dominantly composed of shale. Lithologically, it consists of hard-platy shales, siltstones and fine-grained sandstones with coarsening upward cycles. Fossils and sedimentary structures preserved in this interval are mainly mudcracks and trace fossils. It also contains stromatolites, ostracodes, conchostracans, tetrapod teeth, dinosaur tracks and fish debris. The bedding pattern is interpreted as being representative of varying climatic cycles (Kirkland et al., 2014). It also is interpreted as a shift towards a distal environment within the photic zone of the lake.

3. BIOSTRATIGRAPHY

Palynomorph, conchostracan, and ichnofossil studies have all yielded different biostratigraphic results in determining a relative age for the Moenave Formation (Figure 10). Cornet and Waanders (2006) conducted a palynomorph study of the Whitmore Point Member and upper Dinosaur Canyon Member of the Moenave Formation and concluded that the middle

Whitmore Point Member was mid to late Hettangian (early Jurassic) in age. This relative age was based upon the correlation of palynoflorules in the upper Dinosaur Canyon Member and the middle Whitmore Point Member to *Classopollis meyerianus* and *Classopollis torosus* of the Portland Formation in the Newark Supergroup (Cornet and Waanders 2006). *Classopollis meyerianus* Palynofloral Zone is confined within the Newark Supergroup by the Zone of Extrusives which Ar geochronology and U-Pb zircon dating have yielded an age of 201 $\pm$ 1 Ma.

Conchostracan biostratigraphy conducted by Lucas et al., 2011, yielded the possible location of the Triassic – Jurassic boundary within the upper portion of the Whitmore Point Member approximately 1 kilometer west of the Whitmore Point Reference Section. The Triassic – Jurassic was defined by Lucas et al., 2011, as a co-occurrence of *Euestheria brodieana* and *Bulbilimnadia killianorum.* This co-occurrence occurs approximately 3 meters below the unconformable contact with the Springdale Sandstone of the Kayenta Formation. This conchostracan co-occurrence has also been correlated to conchostracan zones within lower Jurassic strata in the Holy Cross Mountains, Poland and the Midland Formation in the Newark Supergroup. Kozur and Weems, 2010, state that the *Bulbilimnadia killianorum* Zone starts at a continental level no lower than the marine ammonoid *Psiloceras spelae* Zone thus indicating a correlation between marine and terrestrial strata. This provides a strong argument for the location of the Triassic – Jurassic boundary to be within the Whitmore Point Member.

The upper Dinosaur Canyon and Whitmore Point members have yielded numerous amounts of *Eubrontes* and *Grallator* dinosaur tracks (Milner et al., 2012). These two tracks indicate a post end-Triassic extinction (late Triassic) to early Jurassic age for the Whitmore Point Member and upper Dinosaur Canyon Member. However, recent findings of *Anomepus* tracks, known to be exclusively post-end-Triassic to early Jurassic, in the lower Whitmore Point

Member at the Whitmore Point Reference Section and St. George Dinosaur Discovery Site suggest a post end-Triassic extinction to early Jurassic age (Milner et al., 2012), and that the end-Triassic extinctions occurs in the lower part of the Whitmore Point Member and the Triassic-Jurassic boundary occurs in the upper Whitmore Point Member. However, considering the diachronous nature of the Whitmore Point-Dinosaur Canyon lithology, using tracks as the sole biostratigraphic indicator has resulted in ambiguous findings, highlighting the importance of using a global stratigraphic indicator such as C-isotope chemostratigraphy to solve these problems.

III. CASE STUDY

A. INTRODUCTION

Earth's climate is controlled to a degree over geologic time by the flux of atmospheric gases, specifically greenhouse gases such as carbon dioxide (CO_2) and methane CH_4 (Cotton and Sheldon 2012). The release of volcanogenic CO_2 and the dissociation of methane hydrates from the emplacement of large igneous provinces (LIPs) have been correlated to global warming and ocean anoxic events throughout geologic time (Wignall 2001). LIPs, specifically continental flood basalts, have the ability to directly control or perturb the Earth's climate through the emission of CO_2 (Schaller et al., 2011) and the dissociation of methane (CH_4) hydrates. An influx of isotopically light carbon (^{12}C) into the oceanic and atmospheric reservoirs due to the emplacement of LIPs causes large negative carbon isotope excursions (NCIEs) in the rock record. Isotopic analysis of sedimentary organic matter ($\delta^{13}C_{organic}$) to identify carbon isotope excursions in marine and terrestrial environments has become a key tool in correlating global carbon cycle perturbations to events that occur within the biosphere (Saltzman and Thomas 2012). The emplacement of the more voluminous LIPs have been correlated to mass extinction

events (Wignall 2001). Isotopic excursions are associated with major extinction events of the Phanerozoic, indicating a causal relationship between biotic and environmental perturbations (Palfy et al., 2001, Hallam and Wignall 1997). The Mesozoic Era contains three of the most prominent mass extinctions: 1) End-Permian, 2) End-Triassic, and 3) End-Cretaceous. The End-Triassic has remained the least studied of these three mass extinction events.

The Central Atlantic Magmatic Province (CAMP) is one of the most voluminous and aerially extensive LIPs to be emplaced during the Phanerozoic with an estimated volume of 3-11 x 10^6 km^3 and an estimated area greater than 2.5 x 10^6 km^2 (Chapter II, Section D, Figure 6) (Marzoli et al., 1999; McHone 2003; Blackburn et al., 2013). Geochronological age measurements (Ar-Ar, and U/Pb) have constrained the rifting and emplacement of the CAMP to have taken place between 202 – 190 Ma with the main magmatic peak of the CAMP occurring between 201.5 and 200.0 Ma (Nomade et al., 2007; Schoene et al., 2010; Marzoli et al., 2011; Blackburn et al., 2013).

Climatic impacts of the CAMP have been extensively modelled and identified within the rock record. Carbon emissions released as CO_2 and CH_4 during the emplacement of the CAMP are estimated to be ~8,000-9,000 and ~5,000 gigatons respectively (Beerling and Berner 2002). Empirical data obtained from the leaf stomata ratios and pedogenic carbonates have been used to estimate atmospheric CO_2 concentrations during this time. McElwain et al., (1999) used leaf stomata ratios from fossilized Ginkgoalean and Cycadalean leaves to estimate a change in atmospheric CO_2 concentration from 600 ppm to 2100-2400 ppm across the Triassic – Jurassic boundary. Pedogenic carbonates from the Newark and Hartford basins estimate a change in atmospheric CO_2 concentrations from the pre-eruptive background concentration of 2,000 ppm to ~4,500-5,000 ppm (Schaller et al., 2011, 2012, 2014). Although, stomata ratios and pedogenic

carbonates estimate different concentration levels, they are being affected by the same event and show an increasing trend after emplacement of the CAMP. Mean global temperature changes associated with this abrupt rise in atmospheric CO_2 have been estimated to be 3°- 4°C, with models estimating a potential 6°C increase (McElwain et al., 1999, Huynh et al., 2004). A mean global temperature change of 3° to 6°C would have driven selection amongst terrestrial vegetation to avoid lethal leaf limits aiding in the >95% turnover in megafloral species (McElwain et al., 1999) and may have driven global mass extinction.

The emplacement of the CAMP has been linked to the end-Triassic extinction (Blackburn et al., 2013; Whiteside et al., 2010). The end-Triassic extinction (ETE) is one of the largest mass extinction events of the Phanerozoic era affecting both terrestrial and marine biota (Raup and Sepkoski, 1984). It has been ranked third in ecological-severity (~33-40% loss of marine genera) and second in its taxonomic-severity (73% loss) (McGhee et al., 2013) indicating that it had a large impact to the biodiversity of Earth's biosphere. The ETE is also characterized by a 50% loss of tetrapod species, and a 95% turnover of megafloral species (McElwain et al., 1999). The ETE occurs synchronously (201.564 $\pm$ 0.015/0.22 MYA) with early phases of the emplacement of the CAMP, indicating a cause and effect relationship between the two events (Blackburn et al., 2013; Whiteside et al., 2010), and lasted ~20-40 kya (Ruhl et al., 2009).

Lakes respond rapidly to environmental perturbations due to their smaller chemical residence times than oceans (Hollander and McKenzie, 1991). This enhanced sensitivity to environmental perturbations can record pronounce changes in geochemical cycles during periods when global geochemical cycles are forced out of a steady state. Variations in the carbon isotopic composition of terrestrial organic matter and lacustrine carbonates can help identify changes in the global carbon cycle and in atmospheric CO_2 (Kump and Arthur, 1998).

This study is the first to document the climatic impacts to terrestrial ecosystems caused by CAMP perturbations to the global carbon cycle in western Pangea. We do this by investigating the lacustrine Whitmore Point Member (WPM) of the Moenave Formation located in southwestern Utah and northern Arizona. The Whitmore Point Member of the Moenave Formation is a key link to understanding carbon cycle changes during the late Triassic to early Jurassic. Identifying the pronounce carbon cycle perturbations associated with the CAMP at various sections throughout the WPM will aid in understanding the catastrophic and global effects that the CAMP had on Earth systems. Also, identification of CAMP carbon cycle perturbations also provide a means of correlation amongst terrestrial strata that cannot necessarily be correlated by biostratigraphy or geochronology.

We present carbon isotope chemostratigraphic data that identify perturbations in $\delta^{13}C_{organic}$ and $\delta^{13}C_{carbonate}$ at two regionally distinct stratigraphic locations within the WPM: 1) Potter Canyon, AZ and 2) Warner Valley, UT (Figure 11). $\delta^{13}C_{organic}$ was analyzed at both locations while $\delta^{13}C_{carbonate}$ was analyzed only at the Potter Canyon locality. $\delta^{13}C_{organic}$ was analyzed from the bulk composition of sedimentary terrestrial organic matter which reflect an equilibrated relationship with $\delta\,^{13}C_{atmosphere}$. $\delta^{13}C_{carbonate}$ analyzed from lacustrine carbonates forms in equilibrium with $\delta^{13}C$ of lake HCO_3^- which trends toward equilibrium with $\delta^{13}C_{atm}$ CO_2 (Leng et al., 2004). We find that the atmospheric and environmental effects of the CAMP are global phenomenona that are exhibited in both terrestrial and marine strata. Chemostratigraphic analysis of $\delta^{13}C_{organic}$ and $\delta^{13}C_{carbonate}$ provide evidence for environmental perturbations associated with the CAMP in the lacustrine Whitmore Point Member of the Moenave Formation. The use of stable isotope geochemistry will improve our understanding of carbon cycle responses to terrestrial carbon reservoirs.

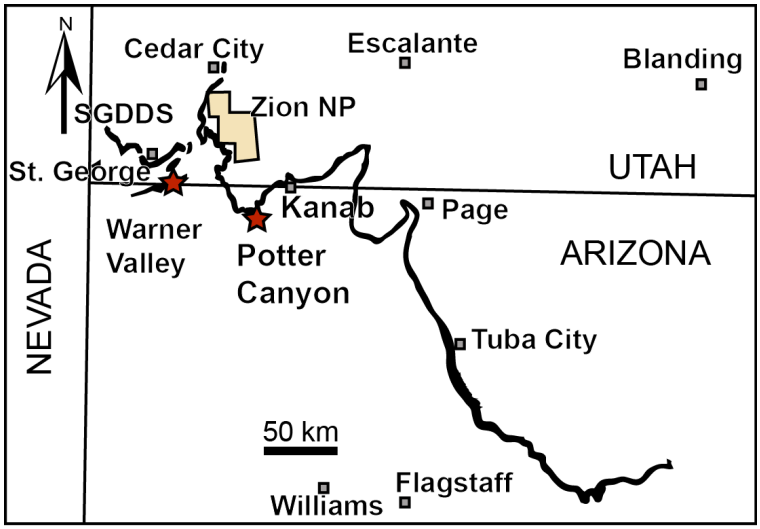

Figure 11. Sample locations (red stars) relative to the Moenave outcrop belt (thick black line). Image modified from Kirkland et al., 2014

B. GEOLOGIC SETTING

The late Triassic (Rhaetian) to early Jurassic (Hettangian) Moenave Formation of southern Utah and northern Arizona consists of fluvial and lacustrine depositional environments occurring in a retro-arc basin that formed on the western edge of the North American craton as a result of collision with the Cordilleran magmatic arc system (Tanner et al 2009). The Moenave Formation (Chapter II, Section G.2, Figure 10) consists of two primary lithostratigraphic members: 1) the Dinosaur Canyon Member (DCM) and 2) the Whitmore Point Member (WPM) (Tanner and Lucas, 2010; Milner et al., 2012; Kirkland et al., 2014). The basal contact of the Moenave Formation is with the underlying Chinle Formation (Late Triassic). The Kayenta Formation overlies the Moenave Formation and is defined by the J –O' unconformity between the Springdale Sandstone of Kayenta and the Whitmore Point of the Moenave. The Wingate Sandstone is chronostratigraphically related to the Moenave Formation and is representative of an erg. The Kayenta Formation and Wingate Sandstone inter-finger with the Moenave Formation to the northeast of the Moenave outcrop belt.

The Whitmore Point Member represents a shallow perennial lacustrine environment along the north to northwest trending Dinosaur Canyon alluvial system as evident by small stromatolitic mounds, salt and gypsum casts, and abundant mud cracks. The terminal floodplain and occasional flood outs of the Dinosaur Canyon fluvial system provided clastic sediments which comprise the Whitmore Point. The Whitmore Point Member has variable stratigraphic thicknesses along the Moenave outcrop belt but overall has been divided into three distinctive lithologic intervals: 1) a lower shale and sandstone interval, 2) a middle sandstone dominated interval and 3) an upper shale dominated interval (Chapter II, Section G.2, Figure 10). The entire Whitmore Point represents two lake megacycles, a thick lower cycle and a thin upper cycle (bounded by the middle proximal sandstone) that are the remains of an ancient lake termed "Lake Dixie"(Milner et al., 2012).

The lower shale and sandstone interval of the WPM has been divided into two separate packages: 1) a lower shale unit and 2) an upper sandstone unit. The lower unit has been described as a well-laminated, poorly to moderately indurated dark organic and calcareous shale dominated unit. This interval is highly fossiliferous containing well-preserved ostracods, conchostracans; a thin stromatolite layer; and plant fragments and fish debris. The upper sandstone dominated unit consists of a grayish-red silty shale and a thin sandstone layer on top, both of which are unfossiliferous. Lenticular sandstone beds are exhibited at some outcrops of the WPM in this lower sequence. These lenses are meters thick and not laterally extensive. They display large-scale soft-sediment deformation features such as over-steepened rotated bedding, minor folding, and water escape structures. Laminar and trough-cross-bedding occur where the sandstone lenses are not deformed. This lower sequence of the WPM is interpreted as a distal lacustrine environment that was partially in the photic zone of the lake, allowing the formation of

stromatolites. The sandstone lenses in the upper part of this interval are interpreted as channels that formed during periods of reduced depositional base level (Kirkland et al., 2014).

The middle sandstone interval overlies the lower shale and sandstone interval. This interval is dominated by fine to medium grained sandstone beds with interspersed sandy mudstone intervals. Sandstone layers display ripple cross-bedding, mudcracks, burrows and the dinosaur cracks *Grallator* and *Anomepus*. This interval is a cliff-forming portion of the WPM and is interpreted as a migrating sandbar or spit.

The upmost interval of the WPM is the upper shale interval. This interval is described as being dominantly composed of mauve-colored shale. Lithologically it consists of hard platy shales, siltstones and fine-grained sandstones with coarsening upward cycles. Fossil and sedimentary structures preserved in this interval are mainly mudcracks and trace fossils. This interval also consists of stromatolites, ostracodes, conchostracans, tetrapod teeth, dinosaur tracks and fish debris. The bedding pattern is interpreted as being representative shifting depositional environments oscillating between distal portions of the lake to proximal photic zones and edges of the lake representing rapidly varying climatic conditions.

C. STABLE ISOTOPE GEOCHEMISTRY METHODS

Bulk samples of sedimentary rock were collected at three geographically distinct sections were measured and sampled for geochemical analysis: 1) Potter Canyon, AZ, and 2) Warner Valley, UT. 37 samples were collected at Potter Canyon at arbitrary intervals. 56 samples were collected from Warner Valley at a sampling frequency of ~30 cm. 93 total samples were collected from the Whitmore Point Member for both organic carbon and inorganic carbonate isotope analysis.

Two geochemical methods were used to analyze $\delta^{13}C$ to develop organic carbon and inorganic carbonate isotope curves. Instrument stability, accuracy and precision were monitored via standard analysis. To obtain bulk $\delta^{13}C_{organic}$, samples were crushed into a fine powder with a mortar and pestle and prepared for decarbonation. A modified decarbonation method followed that of Suarez et al., (2013). 30 mL of 3M HCl was added to ~ 1 gram of sample and reacted for ~2 – 4 hours or until the reaction went to completion. Samples were then rinsed to neutrality with DI water, dried, and crushed. 15.5-16.5 mg of crushed sample was then weighed for analysis on a ThermoFinnigan Delta Plus isotope ratio mass spectrometer (IRMS) via combustion in an elemental analyzer at the University of Arkansas Stable Isotope Laboratory. $\delta^{13}C_{organic}$ was recorded in per mil (‰) relative to VPDB (Vienna Pee Dee Belemnite) and was calculated with the use of laboratory standards. Internal laboratory standards include Black Weeks (-25.04 ± 0.61, actual = -24.74, material standard); Corn Maise (-11.33 ± 0.11, actual = -11.32, high standard); and White River Trout (-26.60 ± 0.15, actual = -26.63, low standard). Other standards used were Peach leaf 1547 (-25.82 ± 0.02, actual = -25.76), and Sucrose ANU (-10.46 ± 0.05, actual = -10.4).

$\delta^{13}C_{carbonate}$ was analyzed from the initial crushed sample. ~0.5 mg of sample was weighed on a Sartorius microbalance into a 12.5mL Exetainer vial, flushed with helium, and dissolved in phosphoric acid to liberate $\delta^{13}C_{carbonate}$ in the form of CO_2 gas. CO_2 gas was equilibrated at 25°C for 18 hours. CO_2 gas was then extracted via a gas bench connected to a ThermoFinnigan Delta Plus IRMS. $\delta^{13}C_{carbonate}$ was recorded in per mil (‰) relative to VPDB using standard δ notation and was calculated using the laboratory standard NBS-19 (1.94 ± 0.13).

The stratigraphic location of each sample within the WPM was plotted against $\delta^{13}C_{organic}$ and $\delta^{13}C_{carbonate}$ to construct a carbon isotope curve for each measured section. Correlations were

made among the sample sites to corroborate trends in the carbon isotope excursions for $\delta^{13}C_{organic}$ and $\delta^{13}C_{carbonate}$. Data analysis was done with the Pandas data analysis package in the programming language Python.

D. RESULTS

Stable isotope results for Potter Canyon, AZ and Warner Valley, UT are illustrated in Figure 12. See supplemental materials for supporting data. The Potter Canyon carbon isotope curve is composed of 37 measurements taken at random intervals over 26.4 m of section. Potter Canyon $\delta^{13}C_{organic}$ values ranged between a minimum of -30.26‰ and a maximum of -23.22‰ with an average of -25.38‰. A distinct 5.5‰ negative carbon isotope excursion (NCIE) occurs from 9.86 m to 11.29 m with a minimum value (-30.26‰) at 10.6 m. This NCIE is followed by a positive carbon isotope excursion (PCIE) from 11.57 m to 13.95 m with a maximum value of -23.22‰. A second subtle NCIE with a minimum of -26.23‰ is seen from 14.66 m to 26.44 m. This NCIE does contain a very small PCIE from 19.31 to 19.8 m with a maximum value of -24.34‰. Relative-total organic carbon is the percent of TOC in a decarbonated sample, rather than the true %TOC which includes the mass of C from carbonate, which was removed during decarbonation of the samples. Relative-total organic carbon (%) is generally low through the Potter Canyon section and ranges from a minimum of 0.02% to a maximum of 0.31%. Relative-total organic carbon shows a relationship to $\delta^{13}C_{organic}$ at Potter Canyon based off of R^2 and p-value ($R^2 = 0.58$, $p = 5.57 \times 10^{-8}$) (Figure 13). An increase in the amount of organic matter preserved at the location of the NCIE does exist and is discussed in more detail in Chapter III, Section E, Discussion.

Potter Canyon $\delta^{13}C_{carbonate}$ values ranged between a minimum of -6.97‰ and a maximum of -2.77‰ with an average of -5.07‰. A distinct NCIE of 2.75‰ occurs from 9.86 m and 12.92

m with a minimum value of -6.77‰ at 11.06 m (Figure 12). This NCIE is followed by a PCIE from 12.92 m to 15.35 m with a maximum value of -2.77‰. A second NCIE is also seen in $\delta^{13}C_{carbonate}$. This second NCIE shows a trend towards lighter values from 15.35 m to 26.44 m with a minimum value of -6.97‰. Weight-percent $CaCO_3$ preserved at Potter Canyon does not influence the $\delta^{13}C_{carbonate}$ of the samples. Overall, the Potter Canyon section appears to capture the chemostratigraphic record of the CAMP in both the $\delta^{13}C_{organic}$ and $\delta^{13}C_{carbonate}$.

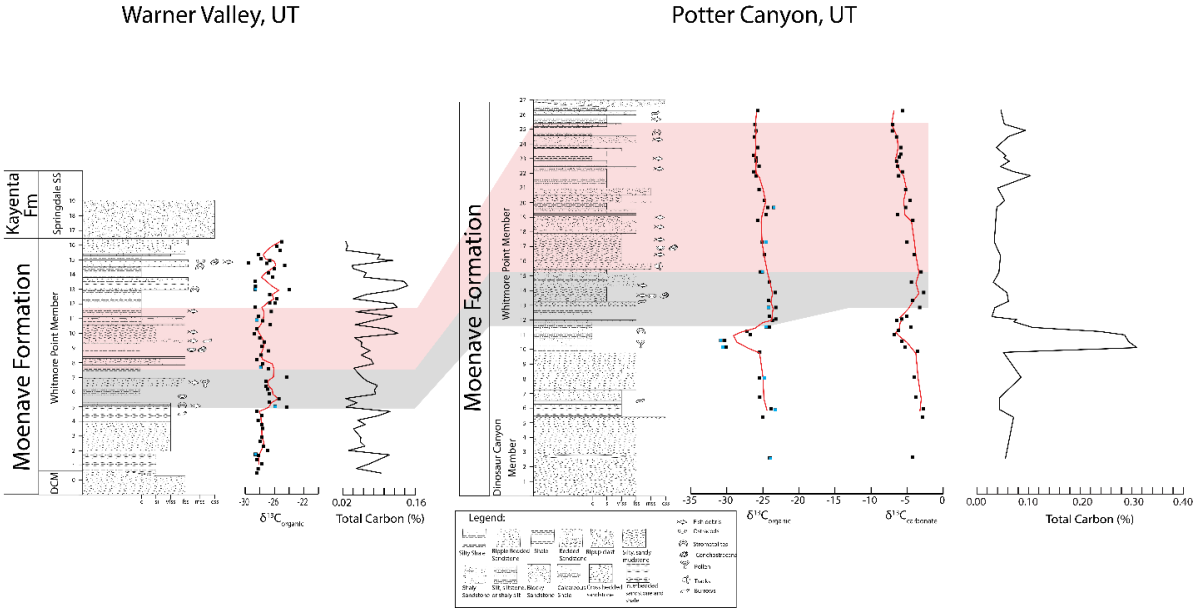

Figure 12: Chemostratigraphic profiles of the Whitmore Point Member. The NCIE that is observed at Potter Canyon is absent from the Warner Valley data set. This distinctive NCIE could be located within the underlying Dinosaur Canyon Member due to its diachronous relationship with the Whitmore Point Member. Red lines represent a 3 point moving average. The initial NCIE, PCIE, and main NCIE that are characteristic of late Triassic carbon isotope curves are preserved within the Whitmore Point Reference Section (Potter Canyon), while the PCIE and main NCIE are both preserved at Warner Valley. Blue squares represent duplicate samples.

Samples from Warner Valley were collected every ~30 cm from the top of the Dinosaur Canyon Member to the base of the Springdale Sandstone of the Kayenta Formation of a 16.325 m interval. Only $\delta^{13}C_{organic}$ was analyzed for Warner Valley because of visible diagenesis in the authigenic carbonate. For example, recrystallization of ostracodes and conchostracans precluded

us from analyzing inorganic carbonate for $\delta^{13}C_{carbonate}$ at Warner Valley without detailed petrographic analysis and microsampling of different carbonate phases. Warner Valley $\delta^{13}C_{organic}$ values ranged between a minimum of -28.72‰ and a maximum of -23.97‰ with an overall average of -27.08‰. The first ~4 m is relatively invariant with $\delta^{13}C_{organic}$ values around ~ -27.5‰. A small PCIE is exhibited from 4.88 m to 6.98 m with a maximum $\delta^{13}C_{organic}$ value of -24.37‰ at 4.88 m and an overall average of -26.04‰. Following the PCIE, a decrease in $\delta^{13}C_{organic}$ values occur from 6.98 m to 11.78 m with a minimum value of -28.72‰ at 9.98 m. $\delta^{13}C_{organic}$ values increase between 11.78 m and 12.97 m with a maximum $\delta^{13}C_{organic}$ value of -23.97‰ at 12.97 m. No distinctive NCIE is observed in the section. A 3-point moving average was calculated to eliminate sample noise and to help identify any overall trends in $\delta^{13}C_{organic}$. Relative-total organic carbon measured at Warner Valley was highly variable, ranging from 0.03% to 0.15%. Relative-total organic carbon indicates a relationship with $\delta^{13}C_{organic}$ based off of R^2 and p-value ($R^2 = 0.26$, $p = 3.55 \times 10^{-4}$) (Figure 13). The relationship between $\delta^{13}C_{organic}$ and relative-total organic carbon (%) is discussed in more detail in Chapter III, Section E, Discussion.

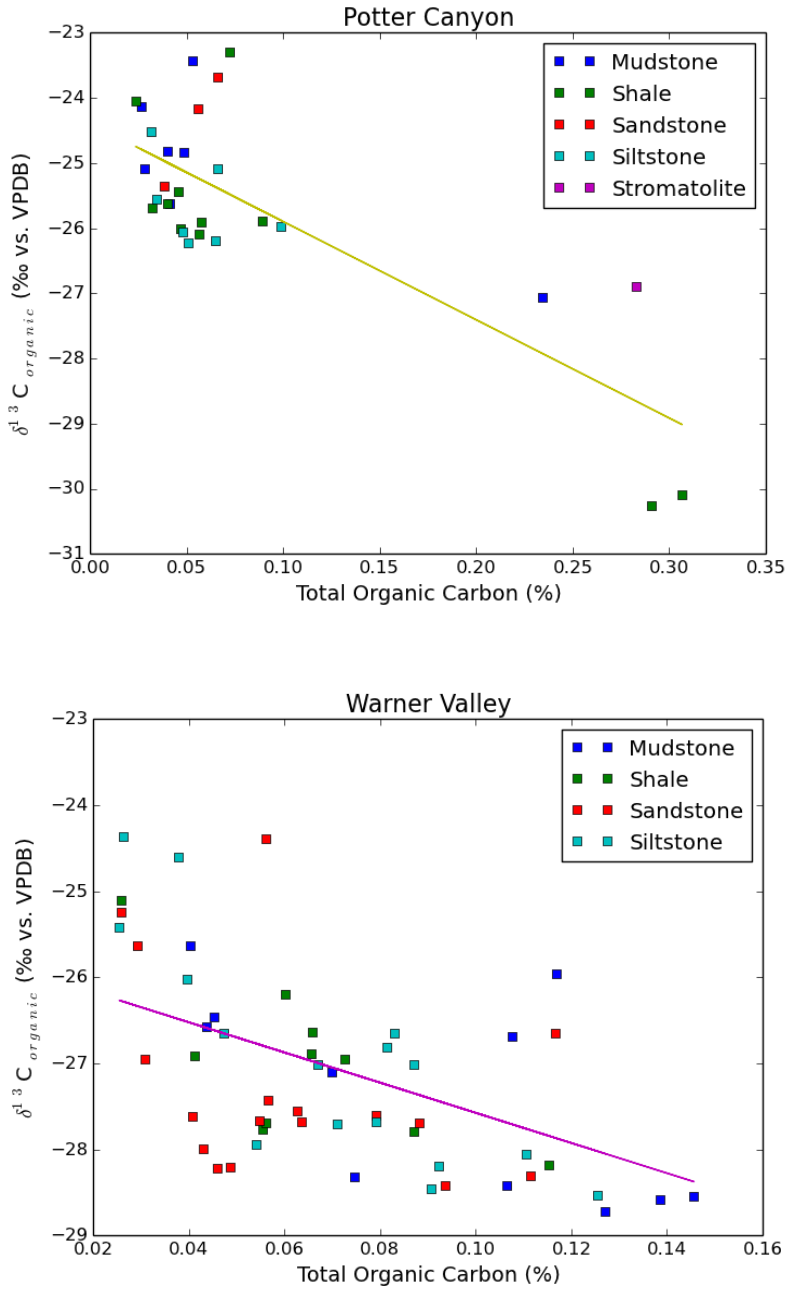

Figure 13. $\delta^{13}C_{organic}$ (‰) vs. relative-total organic carbon (%). All values have been organized by lithology. Lithology does not seem to control the amount of carbon preserved. A relationship between $\delta^{13}C_{organic}$ (‰) and relative-total organic carbon (%) is observed at both localities as indicated by p values; however, low R^2 values indicate that the $\delta^{13}C_{organic}$ (‰) is not a function of the amount of carbon preserved. Potter Canyon: slope = -15.59; intercept = -24.19; r = -0.76; p = 5.57 x 10^{-8}. Warner Valley: slope = -17.678; intercept = -25.82; r = -0.51; p = 5.19x10^{-5}.

E. DISCUSSION

The terrestrial carbon isotope record of western Pangea during the late Triassic is relatively unknown. The focus of most carbon isotope stratigraphy studies through late Triassic to early Jurassic strata has been within or adjacent to the Tethys Ocean (Palfy et al., 2001, Hesselbo et al., 2002; Galli et al., 2005, 2007; Ruhl et al., 2009; Whiteside et al., 2010). Two studies through marine strata have been conducted in western Pangea (Ward et al., 2001; Guex et al., 2004). The initial carbon isotope excursion (ICIE) associated with the Central Atlantic Magmatic Province and the end-Triassic extinction has been documented in these studies and is utilized as a global correlation tool (Figure 14) (Palfy et al., 2001; Ward et al., 2001; Hessselbo et al., 2002; Guex et al., 2004; Palfy et al., 2007; Ruhl et al., 2009, Corso et al., 2014). The magnitude of the ICIE varies amongst different strata with some studies reporting anywhere between a 3-8‰ decrease in $\delta^{13}C$. Hesselbo et al., 2002, showed that the carbon isotope profile of St. Audrie's Bay is characterized by an initial negative carbon isotope excursion of ~5‰ that is succeeded by a PCIE of ~3.5‰ and then a main carbon isotope excursion that transgresses across the Tr-J boundary established by the Global Stratotype Boundary Section and Point (GSSP). The magnitude and distinct characteristic of the St. Audrie's Bay carbon isotope curve has allowed it to become the reference for correlation amongst carbon isotope curves across the Tr-J.

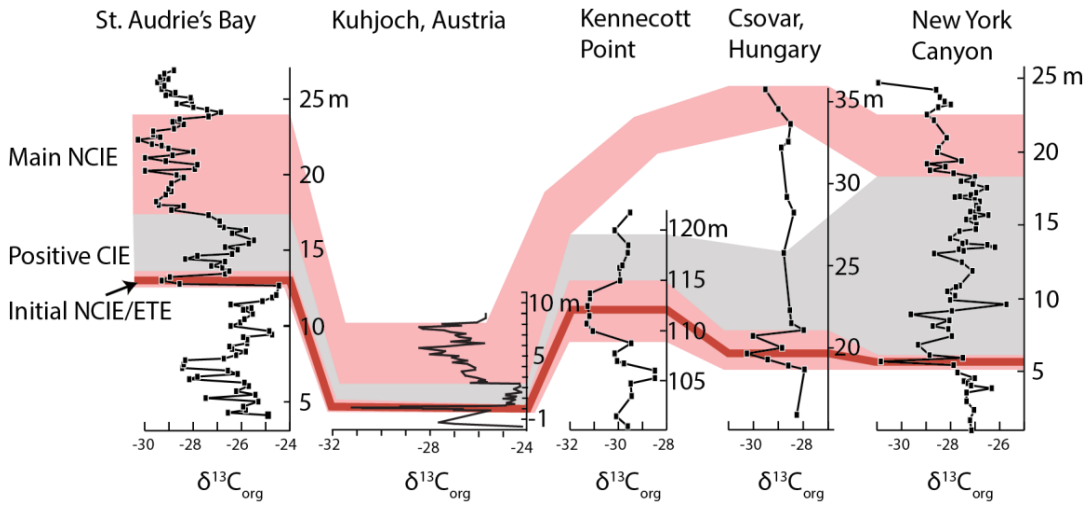

Figure 14. Global carbon isotope stratigraphy trends of the late Triassic to early Jurassic. Most sections are characterized by an initial negative carbon isotope excursions (NCIE) that has been correlated to the end-Triassic extinction (Blackburn et al., 2013). This initial NCIE is followed by a positive carbon isotope excursion which is then followed by a drawn out main NCIE that transgresses the Triassic – Jurassic Boundary. St. Audrie's Bay data is from Hesselbo et al., 2002; Kuhjoch, Austria data is from Ruhl et al., 2009; Kennecott Point data is from Ward et al., 2001; Csovar, Hungary data is from Palfy et al., 2001; New York Canyon data is from Guex et al., 2004.

The excursions exhibited in $\delta^{13}C_{organic}$ and $\delta^{13}C_{carbonate}$ at Potter Canyon, -5.5‰ and -2.75‰ respectively, correlate to the ICIE in previously published studies (Figure 15). This is the first recorded occurrence of a terrestrial carbon cycle perturbation in western Pangea supporting the global nature of emissions from the CAMP affecting both marine and terrestrial environments. Based on studies by Whiteside et al., 2010, and Blackburn et al., 2013, this NCIE should correlate to the ETE indicating a potential cause and effect relationship between the emplacement of the CAMP and the ETE. Schaller et al., 2011, estimated an atmospheric ρCO_2 increase from a pre-eruptive background atmospheric ρCO_2 of ~2,000 ppm to ~4,400 ppm that coincides with the ETE. These atmospheric ρCO_2 values are estimated from pedogenic carbonates formed stratigraphically before, during and after the emplacement of the CAMP. Schaller et al., 2011, has provided a clear trend in an abrupt change in atmospheric ρCO_2 that is

related to the emplacement of the CAMP. A rise of isotopically light atmospheric CO_2 will shift the $\delta^{13}C$ of both organic carbon and carbonate towards lighter values. Therefore, an increase in the amount of carbon preserved in the rock record can be associated with a prominent NCIE.

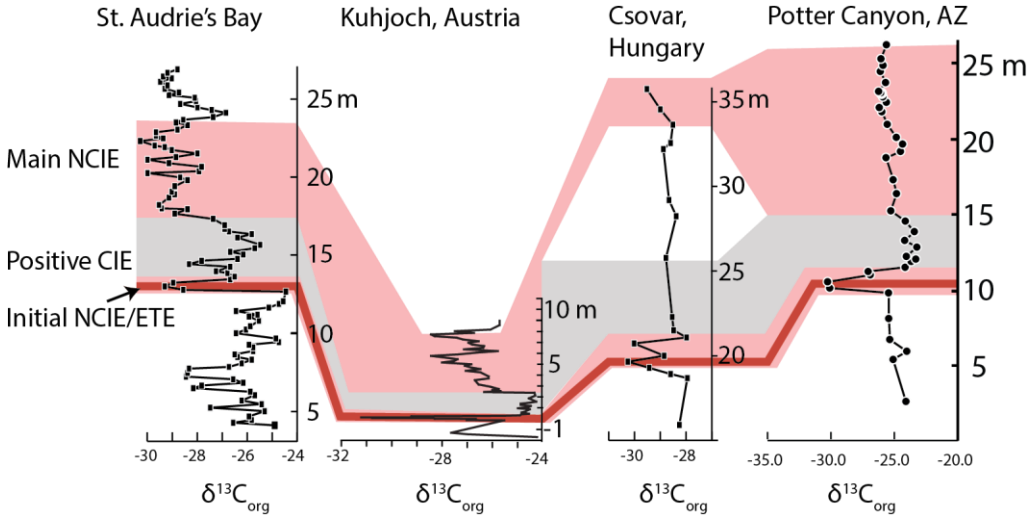

Figure 15. Correlation of $\delta^{13}C_{organic}$ at the Whitmore Point Member Reference Section (Potter Canyon) to the initial NCIE found at St. Audrie's Bay, UK (Hesselbo et al., 2002); Kuhjoch, Austria (Ruhl et al., 2009); and Csovar, Hungary (Palfy et al., 2001). Correlation of the initial NCIE indicates that the CAMP induced a global carbon cycle perturbation in both marine and terrestrial environments.

An increase in atmospheric CO_2 results in an increase in photosynthesis. This increase in the rate of photosynthesis due to CO_2 enrichment leads to an increase in biomass (Beerling and Woodward, 1995). McElwain et al., 1999, estimated a global temperature increase of 3-4°C. An increase in temperature also can increase the rate of photosynthesis by expediting biochemical processes associated with photosynthesis. The $\delta^{13}C_{organic}$ will become depleted in relation to $\delta^{13}C_{atmosphere}$ as bioproductivity increases in response to rising temperatures and rising atmospheric ρCO_2. This depletion in $\delta^{13}C_{organic}$ is the result of a larger and isotopically lighter atmospheric CO_2 reservoir that overall leads to greater kinetic fractionation in organisms due to an increase in photosynthesis amongst photosynthesizing organisms. This could explain why an

observed decrease in $\delta^{13}C_{organic}$ corresponds to an increase in the amount of carbon preserved in the sediment at the Potter Canyon locality.

The CO_2 reservoir will decrease resulting in the utilization of more ^{13}C once the rate of photosynthesis overcomes the rate of CO_2 replenishment (Hollander and McKenzie 1999). This will result in a PCIE. As bioproductivity increases in response to rising temperatures and rising atmospheric CO_2 a drawdown in atmospheric CO_2 can be observed. Rapid burial and sequestration of ^{12}C during periods of high bioproductivity can cause a depletion of ^{12}C in the carbon pool resulting in a greater abundance of ^{13}C. More ^{13}C is readily available and used therefore showing an enrichment in $\delta^{13}C_{organic}$ and $\delta^{13}C_{carbonate}$. This increase in both the $\delta^{13}C_{organic}$ and $\delta^{13}C_{carbonate}$ reservoirs results in a PCIE that follows the initial NCIE, as seen prominently at Potter Canyon.

Intuition would suggest that during an increase in bioproductivity, the $\delta^{13}C_{carbonate}$ would become enriched due to less ^{12}C in the system; however, the $\delta^{13}C_{carbonate}$ curve shows a decrease in $\delta^{13}C$ rather than an increase. This decrease can be explained by the combination of two scenarios: 1) Replenishment of isotopically light carbon from atmospheric CO_2 into the lacustrine system was greater than bioproductivity; therefore, decreasing the $\delta^{13}C_{carbonate}$ in relation to the $\delta^{13}C_{atmosphere}$; and 2) decomposition and oxidation of organic matter sediment during periods of increased bioproductivity would result in isotopically light carbon (~ -15‰ to -20‰) as $CO_{2(aq)}$ (Hollander and McKenzie 1991, Leng et al., 2004, Breugel 2006). An increase in $CO_{2(aq)}$ from decomposing organic matter will result in a decrease of $\delta^{13}C$ from the dissolved inorganic carbon pool (Leng et al., 2004, Breugel 2006). These two scenarios, under the correct conditions, would cause a concomitant decrease in both $\delta^{13}C_{organic}$ and $\delta^{13}C_{carbonate}$.

Kump and Arthur (1998) modelled the effects of a 50% increase in volcanic CO_2 emissions and concluded that a 50% rise in atmospheric ρCO_2 would cause large NCIEs in both $\delta^{13}C_{organic}$ and $\delta^{13}C_{carbonate}$ with $\delta^{13}C_{organic}$ exhibiting a larger decrease (~2‰) than $\delta^{13}C_{carbonate}$. Kump and Arthur (1998) conclude that a large NCIE in $\delta^{13}C_{organic}$ accompanied by a smaller response in $\delta^{13}C_{carbonate}$ can be indicative of an increase in atmospheric CO_2 from a volcanically derived source. Thus, we suggest that the abrupt $\delta^{13}C$ decrease observed in both the organic and carbonate carbon reservoir is due to an influx of light carbon to the atmosphere during the eruption of the CAMP.

However, while both Potter Canyon $\delta^{13}C_{organic}$ and $\delta^{13}C_{carbonate}$ curves show similar trends there are a few discrepancies. The initial excursion exhibited in $\delta^{13}C_{organic}$ is shorter in duration than $\delta^{13}C_{carbonate}$ at Potter Canyon. Also, the $\delta^{13}C_{carbonate}$ exhibits a more prominent main carbon isotope excursion than $\delta^{13}C_{organic}$ at Potter Canyon. The short duration of the negative excursion in $\delta^{13}C_{organic}$ most likely indicates the point at which carbon fixed through photosynthesis overcomes the replenishment of isotopically light $CO_{2(aq)}$ resulting in organisms fixing more ^{13}C than ^{12}C. The minimum $\delta^{13}C_{carbonate}$ value in the carbonate record also lags behind the minimum carbon value in $\delta^{13}C_{organic}$ by 0.46 m. The pH of freshwaters is typically 5.5 – 7. The dominate carbonate species at a lower pH is aqueous CO_2. Biological utilization of $CO_{2(aq)}$ during periods of increased bioproductivity can lower the concentration of $CO_{2(aq)}$. Increasing the amount and rate of photosynthesis decreases the amount of $CO_{2(aq)}$ without an equivalent decrease in alkalinity (Hollander and Mckenzie, 1991). This results in an increase in the carbonate ion concentration, thus leading to the precipitation of carbonates (Hollander and McKenzie, 1991). The $\delta^{13}C_{carbonate}$ values during the NCIE correspond to a slight increase in $CaCO_3$. The minimum $\delta^{13}C_{carbonate}$ during the NCIE is a stromatolite layer. Stromatolites grow in waters where TDIC is

primarily controlled by isotopic exchanges with atmospheric CO_2 and by photosynthesis (Casanova et al., 1993). Stromatolites provide evidence for a decrease in $CO_{2(aq)}$ and an increase in the carbonate ion concentration allowing for the precipitation of carbonate rich layers. The depleted $\delta^{13}C$ values of the stromatolites provide evidence for an isotopically light atmosphere that can be linked to the emissions of the CAMP. The lag seen between the minimum values observed in $\delta^{13}C_{organic}$ and $\delta^{13}C_{carbonate}$ indicates that "Lake Dixie" had a pH in which $CO_{2(aq)}$ was the dominant carbon species. The lag between $\delta^{13}C_{organic}$ and $\delta^{13}C_{carbonate}$ also indicates the point at which bioproductivity utilized enough $CO_{2(aq)}$ to promote carbonate deposition by increasing carbonate ion concentrations. Also, when $CO_{2(aq)}$ is less than 10 μmols, aquatic organisms can preferentially utilize HCO_3^- during photosynthesis; therefore, enriching $\delta^{13}C_{organic}$ and resulting in a PCIE.

No distinct NCIE is found within the Warner Valley section; however, due to the ephemeral deposition of the Whitmore Point Member and its diachronous contact with the Dinosaur Canyon Member, the ICIE found at Potter Canyon may be located within the underlying Dinosaur Canyon Member; therefore, the initial NCIE observed at Potter Canyon is possibly may not be preserved in the Whitmore Point at Warner Valley but preserved in the underlying Dinosaur Canyon Member. The diachronous relationship between the Dinosaur Canyon Member and Whitmore Point Member could indicate that Warner Valley is preserving the positive carbon isotope excursion and main carbon isotope excursion that Hesselbo et al., 2002, identified as occurring after the initial isotope excursion.

Overall the average value of the Warner Valley $\delta^{13}C_{organic}$ is lighter than the Potter Canyon values (average Warner Valley $\delta^{13}C_{organic}$ = -27.08‰ *versus* average Potter Canyon $\delta^{13}C_{organic}$ = -25.38‰). Another explanation for the light $\delta^{13}C$ values at Warner Valley could be

the result of oxidation and diagenesis of organic matter and carbonate minerals that may have distorted primary isotopic signals. Selective preservation of organic matter during burial will tend to preserve lipids isotopic signature which tends to be lighter in isotopic composition compared to the rest of the organism. Oxidation and diagenesis of organic matter has been shown to decrease the $\delta^{13}C$ of organic matter by up to 1.6‰ within the first 120 days of burial (Lehmann et al., 2002); however, even though oxidation of organic matter may play a role in the overall isotopic composition of organic carbon at Warner Valley, the oxidation should take place in the section as a whole, and not selectively alter or eliminate excursions.

Organic matter preservation at Warner Valley is not dependent upon lithology indicating that organic matter was not selectively oxidized. Likewise at Potter Canyon, the NCIE is unlikely the result of selective oxidation of a particular layer or lithology because there is no correlation to the relative-total carbon (%) relative to the lithologic type (Figure 13). Low p-values and $R^2 >$ 0.50 values suggest that there is a correlation between organic matter and $\delta^{13}C_{organic}$ because $\delta^{13}C_{organic}$ is calculated from the relative-amount of organic matter preserved. However, R^2 values are not much greater than 0.50, suggesting that approximately half of $\delta^{13}C_{organic}$ value is explained to an increase in the amount of organic matter preserved. The Potter Canyon NCIE corresponds to an increase in preserved organic matter which can indicates that the NCIE is a result of an increase in organic matter burial and preservation; however, no concomitant PCIE exists in $\delta^{13}C_{carbonate}$, rather a NCIE exists. The existence of a NCIE in both $\delta^{13}C_{organic}$ and $\delta^{13}C_{carbonate}$ indicates that both carbon reservoirs are driven by atmospheric changes, and the increase in the amount of preserved organic carbon associated with the NCIE is a result of increase bioproductivity. Pending additional analysis of the underlying Dinosaur Canyon

Member at Warner Valley, we interpret the majority of the isotope record at Warner Valley to correlate to the MCIE of other C-isotope records.

F. IMPLICATIONS

The carbon isotope curves exhibited within Potter Canyon follows the characteristics of the carbon isotope curves that encompass the ETE and Tr-J in various sections (Figure 15). The Warner Valley, while not as distinct as Potter Canyon, shows some correlation to the PCIE and MCIE, but could have been influenced by post depositional diagenesis. The correlation of the Potter Canyon NCIE to the ICIE is the first terrestrial evidence of the CAMP in western Pangea. Correlation of the Potter Canyon NCIE to the ICIE suggests that the ETE occurs near the base of the Whitmore Point Member of the Moenave Formation at Potter Canyon, and the Tr-J boundary should be located in the upper Whitmore Point Member. Findings of co-existing conchostracans *Euestheria brodieana* (Rhaetian) and *Bulbilimnadia killianorum* (Hettangian) in the upper part of the Whitmore Point near the Whitmore Point Reference Section (Potter Canyon) indicate the location of the Triassic – Jurassic boundary in terrestrial strata (Lucas et al., 2011). Correlation of the NCIE within the Potter Canyon section to the ETE, based off of Blackburn et al., (2013) correlation, indicates that the fossils found after the NCIE in Potter Canyon are post ETE.

Identification of these carbon isotope curves at different sections within the Whitmore Point Member also help rectify regional correlation issues within the WPM. The carbon isotope excursions provide a basis for correlating different WPM sections that do not contain distinct lithologic packages or key marker beds that would traditionally be used for stratigraphic correlation. Therefore, using the carbon isotope curve from the Whitmore Point Reference Section (Potter Canyon) provides a basis for the carbon isotope curves to be found within other sections of the Whitmore Point Member.

IV. CONCLUSIONS

Carbon isotope chemostratigraphy of the Whitmore Point Member of the Moenave Formation at Potter Canyon and Warner Valley record the preservation of the atmospheric carbon cycle perturbation caused by the CAMP. The well-defined carbon isotope curve in both the $\delta^{13}C_{organic}$ and $\delta^{13}C_{carbonate}$ reservoirs at the Whitmore Point Reference Section (Potter Canyon) exhibit all three characteristics that define the St. Audrie's Bay carbon isotope curve. The correlation of the Potter Canyon carbon isotope curves provide evidence that the CAMP caused a global carbon cycle perturbation that is prominently seen within terrestrial strata. The carbon isotope excursion exhibited at Potter Canyon is the first record of the CAMP carbon cycle perturbation on terrestrial strata.

Chemostratigraphic correlation of the carbon isotope curves within the WPM to other published late Triassic to early Jurassic carbon isotope curves suggest that the lower part of the WPM at Potter Canyon is indeed of late Triassic age and the Triassic-Jurassic boundary is in the upper WPM. The correlation of the initial NCIE with the NCIE found at Potter Canyon in both the $\delta^{13}C_{organic}$ and $\delta^{13}C_{carbonate}$ reservoirs indicates that the ETE is present within the WPM, and that fossil assemblages (tracks, conchostracans, ostracodes etc.) are indicative of being late Triassic. The global correlation of the Potter Canyon NCIE along with the finding of co-occuring conchostracans *Euestheria brodieana* (Rhaetian) and *Bulbilimnadia killianorum* (Hettangian) by Lucas et al., 2011 provide evidence for the location of the Triassic/Jurassic boundary within the upper part of the WPM at Potter Canyon.

The prominent carbon isotope curve associated with the late Triassic is distinctive enough to be used for regional correlation amongst strata that is lacking key marker beds for traditional stratigraphic correlation or where an absolute date cannot be provided. Chemostratigraphic

correlation of the Whitmore Point Member of the Moenave Formation shows the diachronous relationship between the WPM and the DCM. This is illustrated by the correlation of the Potter Canyon carbon isotope curve to the Warner Valley carbon isotope curve. Only the main CIE is preserved in the WPM at Warner Valley, indicating that in that location, the majority of the WPM is of post ETE and likely, early Jurassic in age. Chemostratigraphy of the WPM aids in a better understanding of the age and correlation of the WPM both regionally and globally.

V. REFERENCES

Allen, M. R., Frame, D. J., Huntingford, C., Jones, C. D., Lowe, J. A., Meinshausen, M., Meinshausen, N., 2009, Warming caused by cumulative carbon emissions towards the trillionth tonne: Nature, v. 458, p. 1163-1166, doi: 10.1038/nature08019

Bacon, K. L., Belcher, C. M., Hesselbo, S. P., McElwain, J. C., 2011, The Triassic-Jurassic boundary carbon-isotope excursions expressed in taxonomically identified leaf cuticles: Palaios, v. 26, pp. 461-469, doi: 10.2110/palo.2010.p10-120r

Beerling, D. J., Woodward, F. I., 1995, Leaf stable carbon isotope composition records increased water-use efficiency of C_3 plants in response to atmospheric CO_2 enrichment: Functional Ecology, v. 9, pp. 394-401.

Beerling, D. J., Berner, R. A., 2002, Biogeochemical constraints on the Triassic-Jurassic boundary carbon cycle event: Global Biogeochemical Cycles, v. 16,No. 3,p. 101-13.

Beutal, E. K., Nomade, S., Fronabarger, A. K., Renne, P. R., 2005, Pangea's complex breakup: A new rapidly changing stress field model: Earth and Planetary Science Letters, v. 236, pp. 471-485

Bond, D.P.G., and Wignall, P.B., 2014, Large igneous provinces and mass extinctions: An update, *in* Keller, G., and Kerr, A.C., eds., Volcanism, Impacts, and Mass Extinctions: Causes and Effects: Geological Society of America Special Paper 505, p. 29–55, doi:10.1130/2014.2505(02)

Blackburn, T., Olsen P.E., Bowring S.A., McLean N.M., Kent D.V., Puffer J., McHone G., Rasbury E.T., Et-Touhami M., 2013, Zircon U-Pb geochronology links the end-Triassic extinction with the Central Atlantic Magmatic Province, Science, DOI: 10.1126/science.1234204

Bonis, N. R., Kurschner, W. M., 2012, Vegetation history, diversity patterns, and climate change across the Triassic/Jurassic boundary: Paleobiology, v. 38, pp. 240-264

Breugel, Y.V., 2006, Causes for negative carbon isotope anomalies in Mesozoic marine sediments: Constraints from modern and ancient anoxic settings: Mededelingen van de Faculteit Geowetenschappen Universiteit Utrecht, No. 258 isbn: 10: 90-5744-122-5

Bryan, S., Ernst, R., 2007, Revised definition of large igneous province (LIP): Earth – Science Reviews, DOI: 10.1016/j.earscirev.2007.08.008

Burkhardt, S., Riebesell, U., Zondervan, I., 1999, Effects of growth rate, CO_2 concentration, and cell size on the stable carbon isotope fractionation in marine phytoplankton: Geochimica et Cosmochimica, v. 63, pp. 3729-3741

Caldeira, K., Wickett, M. E., 2003, Anthropogenic carbon and ocean pH: Nature, v. 425, p. 365

Casanova, J., Hillaire-Marcel, C., 1993, Carbon and oxygen isotopes in African lacustrine stromatolites: Palaeohydrological interpretation: Geophysical Monograph, v. 78, pp. 123-133

Ciais, P., C. Sabine, G. Bala, L. Bopp, V. Brovkin, J. Canadell, A. Chhabra, R. DeFries, J. Galloway, M. Heimann, C. Jones, C. Le Quéré, R.B. Myneni, S. Piao and P. Thornton, 2013: Carbon and Other Biogeochemical Cycles. In: Climate Change 2013: The Physical Science Basis. Contribution of Working Group I to the Fifth Assessment Report of the Intergovernmental Panel on Climate Change [Stocker, T.F., D. Qin, G.-K. Plattner, M. Tignor, S.K. Allen, J. Boschung, A. Nauels, Y. Xia, V. Bex and P.M. Midgley (eds.)]. Cambridge University Press, Cambridge, United Kingdom and New York, NY, USA.

Cornet, B., Waanders, G., 2006. Palynomorphs indicate Hettangian (Early Jurassic) age for the middle Whitmore Point Member of the Moenave Formation, Utah and Arizona. New Mexico Museum of Natural History and Science Bulletin 37, 390–406.

Corso, J. D., Marzoli, A., Tateo, F., Jenkyns, H. C., Bertrand, H., Youbi, N., Mahmoudi, A., Font, E., Buratti, N., Cirilli, S., 2014, The dawn of CAMP volcanism and its bearing on the end-Triassic carbon cycle disruption: Journal of the Geological Society, London, v. 171, pp. 153-164, doi: 10.1144/jgs2013-063

Cotton, J.M., and Sheldon, N.D., 2012, New constraints on using paleosols to reconstruct atmospheric *p*CO2: Geological Society of America Bulletin, v. 124, no. 9–10, p. 1411–1423.

Craig, H., 1953, The geochemistry of the stable carbon isotopes: Geochimica et Cosmochimica Acta, v. 3, pp. 53-92

Davis, J. D., 1977, Dinosaur Canyon Member of the Triassic Moenave Formation of Southwest Utah: Wyoming Geological Association Guidebook, v. 29, pp. 201-206

Degens, E. T., 1967, Biogeochemistry of stable carbon isotopes, *in* Eglinton, G., Murphy, M. T. J., Organic Geochemistry Methods and Results: Springer-Verlag Berlin Heidelberg, doi: 10.1007/978-3-642-87734-6

Degens, E. T., Guillard, R. R. L., Sackett, W. M., Hellebust, J. A., 1968, Metablic fractionation of carbon isotopes in marine plankton – I. Temperature and respiration experiments: Deep-Sea Research, v. 15, p. 1-9

Deuser, W. G., Degens, E. T., Guillard, R. R. L., 1968, Carbon isotope relationships between plankton and sea water: Geochimica et Cosmochimica Acta, v. 32., pp. 657-660.

Donohoo-Hurley, L. L., Geissman, J. W., Lucas, S. G., 2010, Magnetostratigraphy of the uppermost Triassic and lowermost Jurassic Moenave Formation, western United States: Correlation with strata in the United Kingdom, Morocco, Turkey, Italy, and eastern United States: Geological Society of America Bulletin, doi: 10.1130/B30136.1

Farquhar, G. D., O'Leary, M. H., Berry, J. A., 1982, On the relationship between carbon isotope discrimination and the intercellular carbon dioxide concentration in leaves: Austral. J. Plant Physiol., v. 9, pp. 121-137

Fowell, S.J., and Olsen, P. E., 1995. Time calibration of Triassic/Jurassic microfloral turnover, eastern North America - Reply. Tectonophysics 245: 96-99

Galli, M. T., Jadoul, F., Bernasconi, S. M., Weissert, H., 2005, Anomalies in global carbon cycling and extinction at the Triassic/Jurassic boundary: evidence from a marine C-isotope record: Palaeogeography, Palaeoclimatology, Palaeoecology, v. 216, pp. 203-214

Galli, M. T., Jadoul, F., Bernasconi, S. M., Cirilli, S., Weissert, H., 2007, Stratigraphy and paleoenvironmental analysis of the Triassic-Jurassic transition in the western Southern Alps (Northern Italy): Palaeogeography, Palaeoclimatology, Palaeoecology, v. 244, pp. 52-70

Guex, J., Bartolini, A., Atudorei, V., Taylor, D., 2004, High-resolution ammonite and carbon isotope stratigraphy across the Triassic-Jurassic boundary at New York Canyon (Nevada): Earth and Planetary Science Letters, v. 225, pp. 29-41

Hallam, A., Wignall, P. B., 1997, Mass extinctions and their aftermath: Oxford University Press, 328 p.

Harvey, H. R., Tuttle, J. H., Bell, J. T., 1995, Kinetics of phytoplankton decay during simulated sedimentation: Changes in biochemical composition and microbial activity under oxic and anoxic conditions: Geochimica et Cosmochimica Acta, v. 59, pp. 3367-3377

Hautmann, M., 2004, Effect of end-Triassic CO_2 maximum on carbonate sedimentation and marine mass extinction: Facies, v. 50, pp. 257-261, doi: 10.1007/s10347-004-0020-y

Hesselbo, S.P., Robinson, S.A., Surlyk, F.,Piasecki, S., 2002, Terrestrial and marine extinction at the Triassic-Jurassic boundary synchronized with major carbon-cycle perturbation: a link to initiation of massive volcanism?: Geology, v. 30, no. 3, p. 251-54

Hoefs, J., 2009, Stable Isotope Geochemistry (sixth edition): Springer-Verlag Berlin Heidelberg, 285 p.

Hollander, D. J., McKenzie, J. A., 1991, CO_2 control on carbon-isotope fractionation during aqueous photosynthesis: A paleo-pCO_2 barometer: Geology, v. 19, p. 929-932

Huynh, T. T., Poulsen, C. J., 2005, Rising atmospheric CO_2 as a possible trigger for the end-Triassic mass extinction: Palaeogeography, Paleoclimatology, Palaeoecology, v. 217, p. 223-242, doi: 10.1016/j.palaeo.2004.12.2004

Kirkland, J. I., Milner, A. R. C., Olsen, P. E., Hargrave, J. E., 2014, The Whitmore Point Member of the Moenave Formation in its type area in northern Arizona and its age and correlation with the section in St. George, Utah: Evidence for two major lacustrine sequences: Utah Geological Association, 43, ISBN: 978-0-9800-489-7-1

Kozur, H.W., Weems, R.E., 2010, The biostratigraphic importance of conchostracans in the continental Triassic of the northern hemisphere, Geological Society, 334, 315-417, doi: 10.1144/SP334.13

Kump, L. R., Arthur, M. A., 1998, Interpreting carbon-isotope excursions: carbonates and organic matter: Chemical Geology, v. 161, pp. 181-1198

Lehmann, M. F., Bernasconi, S. M., Barbieri, A., McKenzie, J. A., 2002, Preservation of organic matter and alteration of its carbon and nitrogen isotope composition during simulated and

in situ early sedimentary diagenesis: Geochimica et Cosmochimica Acta, v. 66, pp. 3573-3584

Leng, M. J., Marshall, J. D., 2004, Palaeoclimate interpretation of stable isotope data from lake sediment archives: Quaternary Science Review, v. 23, 811-831, doi:10.1016/j.quascirev.2003.06.012

Leng, M. J., Lamb, A. L., Heaton, T. H. E., Marshall, J. D., Wolfe, B. B., Jones, M. D., Holmes, J. A., Arrowsmith, C., 2005, Isotopes in lake sediments, *in* Leng, M. J, (ed), Isotopes in Palaeoenvironmental Research, Springer, v. 10, pp. 147-184, doi: 10.1007/1-4020-2504-1_04

Lohmann, K. C., 1988, Geochemical patterns of meteoric diagenetic systems and their application to studies of paleokarst: Paleokarst, p.58-80

Lucas, S.G., Tanner, L.H., Donohoo-Hurley, L.L., Geissman, J.W., Kozur, H.W., Heckert, A.B., Weems, R.E., 2011, Position of the Triassic–Jurassic boundary and timing of the end-Triassic extinctions on land: data from the Moenave Formation on the southern Colorado Plateau, USA: Elsevier, v. 302, p. 194-205, doi: 10.1016/j.palaeo.2011.01.009

Masson-Delmotte, V., M. Schulz, A. Abe-Ouchi, J. Beer, A. Ganopolski, J.F. González Rouco, E. Jansen, K. Lambeck, J. Luterbacher, T. Naish, T. Osborn, B. Otto-Bliesner, T. Quinn, R. Ramesh, M. Rojas, X. Shao and A. Timmermann, 2013: Information from Paleoclimate Archives. In: Climate Change 2013: The Physical Science Basis. Contribution of Working Group I to the Fifth Assessment Report of the Intergovernmental Panel on Climate Change [Stocker, T.F., D. Qin, G.-K. Plattner, M. Tignor, S.K. Allen, J. Boschung, A. Nauels, Y. Xia, V. Bex and P.M. Midgley (eds.)]. Cambridge University Press, Cambridge, United Kingdom and New York, NY, USA.

Marshall, J. D., 1992, Climatic and oceanographic isotopic signals from the carbonate rock record and their preservation: Geology Magazine, 129, pp. 143-160

Marzoli, A., Renne, P.R., Piccirillo, E.M., Ernesto, M., Bellieni, G., De Min, A., 1999, Extensive 200-million-year-old continental flood basalts of the Central Atlantic Magmatic Province, Science, 284, pp. 616-618

Marzoli, A., Jourdan, F., Puffer, J. H., Cuppone, T., Tanner, L. H., Weems, R. E., Bertrand, H., Cirilli, S., Bellieni, G., De Min, A., 2011, Timing and duration of the Central Atlantic magmatic province in the Newark and Culpepper basins, eastern U.S.A.: Lithos, v. 2011, pp. 175-188

McElwain, J.C., Beerling, D.J., Woodward, F.I., 1999, Fossil plants and global warming at the Triassic-Jurassic boundary, Science, 285, 1386, doi: 10.1126/science.285.5432.1386

McGhee, G. R., Clapham, M. E., Sheehan, P. M., Bottjer, D. J., Droser, M. L., 2013, A new ecological-severity ranking of major Phanerozoic biodiversity crises: Palaeogeography, Paleoclimatology, Palaeoecology, v. 370, pp. 260-270

McHone, J.G., 2003, Volatile emissions from Central Atlantic Magmatic Province basalts: mass assumptions and environmental change: AGU monograph

McRoberts, C. A., Newton, C. R., 1995, Selective extinction among end-Triassic European bivalves: Geology, v. 23, pp. 102 - 104

Milner, A.R.C., Birthisel, T.A., Kirkland, J.I., Breithaupt, B.H., Matthews, N.A., Lockley, M.G., Santucci, V.L., Gibson, S.Z., Deblieux, D.D., Hurlbut, M., Harris, J.D., Olsen, P. E., 2012, Tracking early Jurassic dinosaurs across the southwestern Utah and the Triassic-Jurassic transition: Nevada State Museum Paleontological Papers

Nomade, S., Knight, K. B., Beutal, E., Renne, P. R., Verati, C., Feraud, G., Marzoli, A., Youbi, N., Bertrand, H., 2007, Chronology of the Central Atlantic Magmatic Province: Implications for the Central Atlantic rifting processes and the Triassic – Jurassic biotic crisis: Palaeogeography, Palaeoclimatology, Palaeocology, v. 244, pp. 326-344.

Ogg, J. C., 2012, Triassic, *in* Gradstein, F., Ogg, J.C., Schmitz, M., Ogg, G., 2012, The geologic time scale 2012: Elsevier

O'Leary, M. H., 1984, Measurement of the isotope fractionation associated with diffusion of carbon dioxide in aqueous solution: The Journal of Physical Chemistry, v. 88, 823-825

O'Leary, M. H., 1988, Carbon isotopes in photosynthesis: Fractionation techniques may reveal new aspects of carbon dynamics in plants: Bioscience, v. 38, pp. 328-336

Palfy, J., Demeny, A., Haas, J., Hetenyi, M., Orchard, M. J., Veto, I., 2001, Carbon isotope anomaly and other geochemical changes at the Triassic-Jurassic boundary from a marin section in Hungary: Geology, v. 29, p. 1047-1050

Park, R., Epstein, S., 1960, Carbon isotope fractionation during photosynthesis: Geochimica et Cosmochimica Acta, v. 21, pp. 110-126

Pederson, O., Colmer, T. D., Sand-Jensen, K., 2013, Underwater photosynthesis of submerged plants – recent advances and methods: Frontiers in Plant Science, v. 4, pp. 1-19

Popp, B. N., Parekh, P., Tilbrook, B., Bidigare, R. R., Laws, E. A., 1997, Organic carbon $\delta^{13}C$ variations in sedimentary rocks as chemostratigraphic and paleoenvironmental tools: Palaeogeography, Paleoclimatology, Palaeoecology, v. 132, pp. 119-132

Popp, B. N., Laws, E. A., Bidigare, R. R., Dore, J. E., Hanson, K. L., Wakeham, S. G., 1998, Effect of phytoplankton cell geometry on carbon isotopic fractionation: Geochimica et Cosmochimica Acta, v. 62, pp. 69-77

Raup, D.M., Sepkoski, J.J., 1984, Periodicity of extinctions in the geologic past: Proceedings of the National Academy of Sciences USA, V. 81, p. 801-805

Romanek, C. S., Grossman, E. L., Morse, J. W., 1992, Carbon isotopic fractionation in synthetic aragonite and calcite: Effects of temperature and precipitation rate: Geochimica et Cosmochimica Acta, v. 56, pp. 419-430

Ruhl, M., Kurschner, W. M., Krystyn, L., Triassic – Jurassic organic carbon isotope stratigraphy of key sections in the western Tethys realm (Austria): Earth and Planetary Science Letters, v. 281, pp. 169-187

Ruiz-Martinez, V. C., Torsvik, T. H., van Hinsbergen, D. J. J., Gaina, C., 2012, Earth at 200 Ma: Global palaeogeography refined from CAMP palaeomagnetic data: Earth and Planetary Science Letters, 331-332, p. 67-79

Sala, O.E., Chapin, F.S., III, Armesto, J.J., Berlow, E., Bloomfield, J., Dirzo, R., Huber-Sanwald, E., Huenneke, L.F., Jackson, R.B., Kinzig, A.,Leemans, R., Lodge, D.M., Mooney, H.A., Oesterheld, M., Poff, N.L., Sykes, M.T., Walker, B.H., Walker, M., Wall, D.H., 2000. Global Biodiversity Scenarios for the Year 2100. Science, 287(5459): 1770-1774.

Saltzman, M. R., Thomas, E., 2012, Carbon isotope stratigraphy, *in* Gradstein, F., Ogg, J.C., Schmitz, M., Ogg, G., 2012, The geologic time scale 2012: Elsevier

Schaller, M.F., Wright, J.D., and Kent, D.V., 2011, Atmospheric *p*CO2 perturbations associated with the Central Atlantic magmatic province: Science, v. 331, no. 6023, p. 1404–1409, doi: 10 .1126 /science .1199011 .

Schaller, M.F., Wright, J.D., Kent, D.V., and Olsen, P.E., 2012, Rapid emplacement of the Central Atlantic magmatic province as a net sink for CO2: Earth and Planetary Science Letters, v. 323-324, p. 27-39, doi:10.1016/j.epsl.2011.12.028

Schaller, M. F., Wright, J. D., Kent, D. V., 2014, A 30 Myr record of Late Triassic atmospheric ρCO_2 variation reflects a fundamental control of the carbon cycle by changes in continental weathering: Geological Society of America Bulletin, doi: 10.1130/B31107.1

Schlesinger, W. H., Bernhardt, E. S., 2013, Biogeochemistry: An Analysis of Global Change: Academic Press, 672 p.

Schoene, B., Guex, J., Bartolini, A., Schaltegger, U., Blackburn, T., 2010, Correlating the end-Triassic mass extinction and flood basalt volcanism at the 100 ka level: Geology, v. 38, pp. 387-390, doi: 10.1130/G30683.1

Suarez, M. B., Ludvigson, G.A., Gonzalez, L.A., Al-Suwaidii, A.H., and You, H-L., 2013, Stable Isotope Chemostratigraphy in Lacustrine Strata of the Xiagou Formation, Gansu Province, NW China: Geological Society of London, v.382, p. 143-155

Talbot, M. R., 1990, A review of the palaeohydrological interpretation of carbon and oxygen isotopic ratios in primary lacustrine carbonates: Chemical Geology (Isotope Geoscience Section), 80, 261-279

Tanner, L. H., Lucas, S. G., 2007, The Moenave Formation: Sedimentologic and stratigraphic context of the Triassic-Jurassic boundary in the Four Corners area, southwestern U.S.A.: Palaeogeography, Palaeoclimatology, Palaeoecology, v. 244, pp. 111-125, doi: 10.1016/j.palaeo.2005.06.039

Tanner, L. H., Lucas, S.G., 2009. The Whitmore Point Member of the Moenave Formation: Early Jurassic dryland lakes on the Colorado Plateau, southwestern USA. Volumina Jurassica 6, 11–21

Tidwell, W.D. and Ash, S.R., 2006, Preliminary report on the Early Jurassic flora from the St. George Dinosaur Discovery Site, Utah: New Mexico Museum of Natural History and Science Bulletin, v. 37, p. 414-420

Van de Schootbrugge, B., Quan, T. M., Lindstrom, S., Puttmann, W., Heunisch, C., Pross, J., Fiebig, J., Petschick, R., Rohling, H. G., Richoz, S., Rosenthal, Y., Falkowski, P. G., 2009, Floral changes across the Triassic/Jurassic boundary linked to flood basalt volcanism: Nature Geoscience, v. 2, pp. 589-594, doi:10.1038/NGEO577

Ward, P. D., Haggart, J. W., Carter, E. S., Wilbur, D., Tipper, H. W., Evans, T., 2001, Sudden productivity collapse associated with the Triassic-Jurassic boundary mass extinction: Science, v. 292, pp. 1148-1151, doi: 10.1126/science.1058574

Whiteside, J.H., Olsen, P.E., Eglinton, T., Brookfield, M.E., Sambrotto, R.N., 2010, Compound-specific carbon isotopes from Earth's largest flood basalt eruptions directly linked to the end-Triassic mass extinction: Proceedings of the National Academy of Sciences USA, v.107, p. 6721-67215

Wignall, P.B., 2001, Large igneous provinces and mass extinctions: Earth-Science Reviews, v. 53, p. 1-33.

Williford, K. H., Ward, P. D., Garrison, G. H., Buick, R., 2007, An extended organic carbon-isotope record across the Triassic-Jurassic boundary in the Queen Charlotte Islands, British Columbia, Canada: Palaeogeography, Palaeoclimatology, Palaeoecology, v. 244, pp. 290-296

VI. APPENDIX

Warner Valley and Potter Canyon lithologic correlation. Correlation is based off of distinctive lithologic packages exhibited at each study sites that correspond to two lake cycles throughout the depositional history of the Whitmore Point Member.

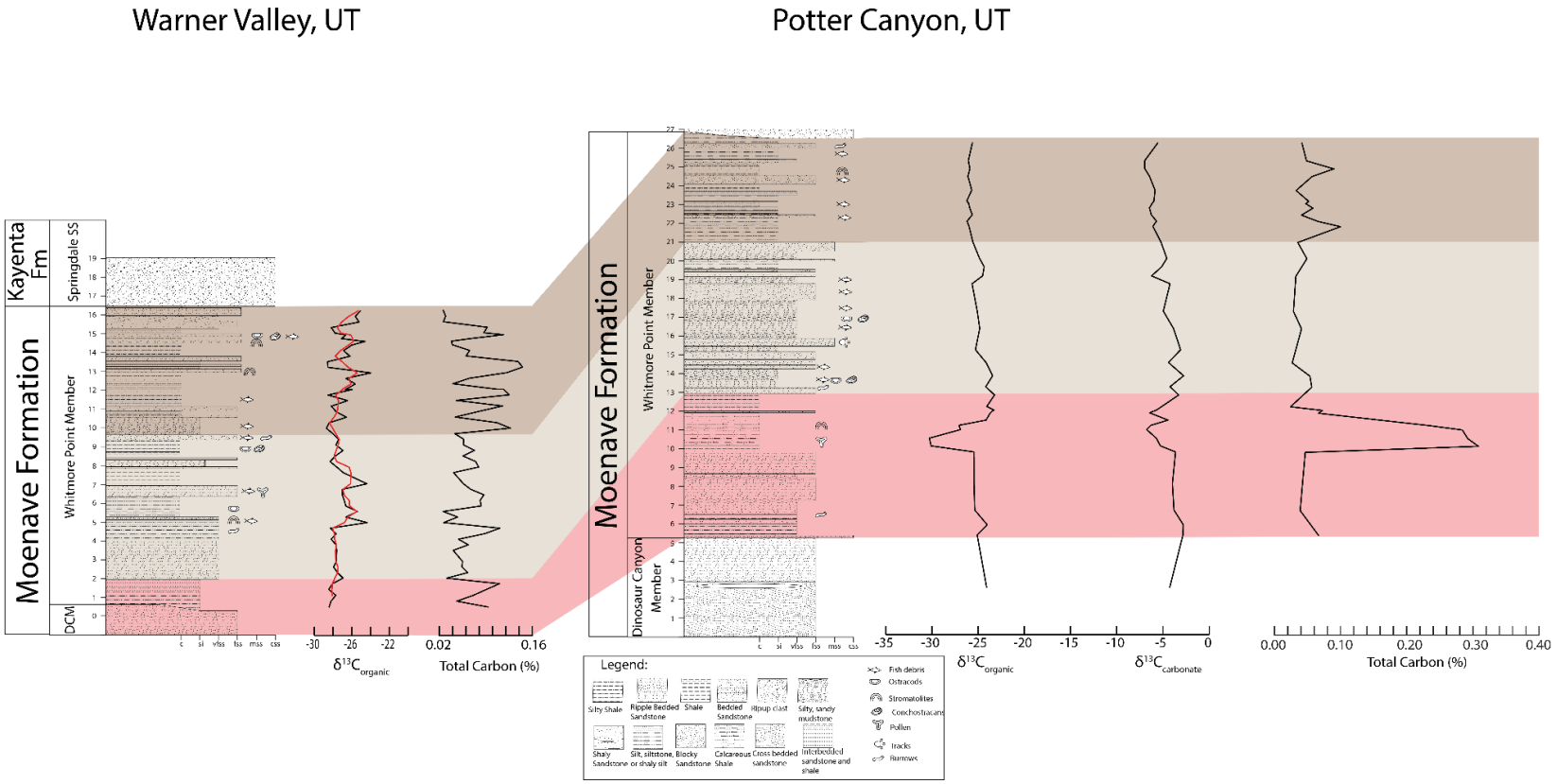

Recrystallized ostracodes from the Warner Valley section. Not visible individual calcite crystals.

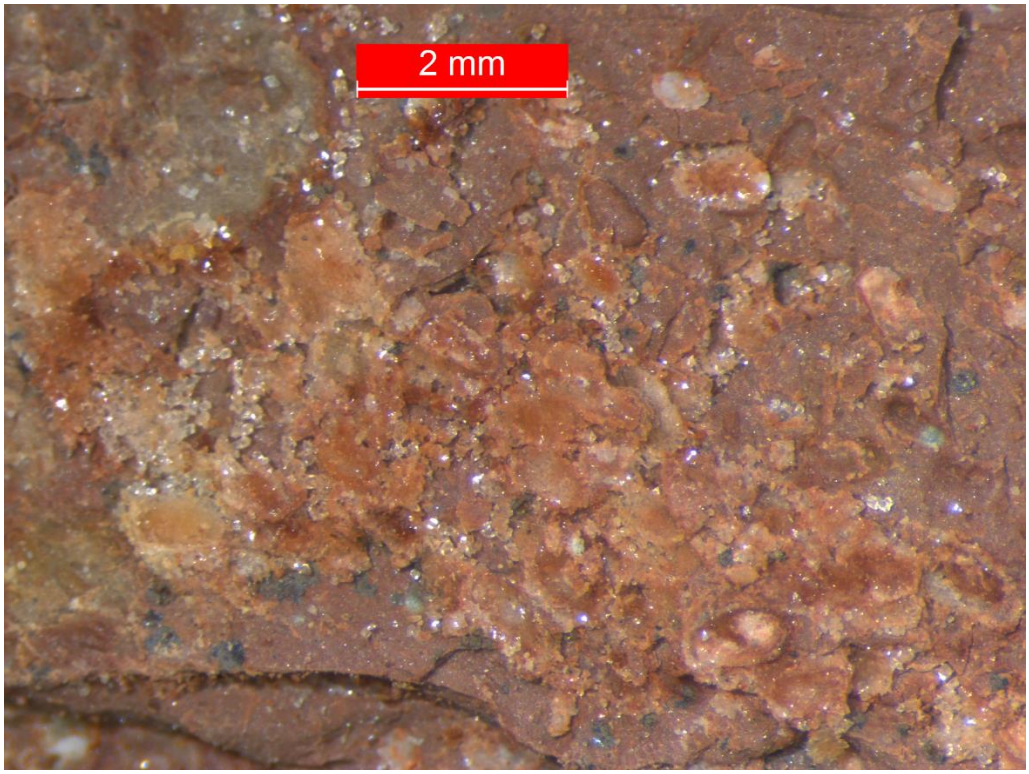

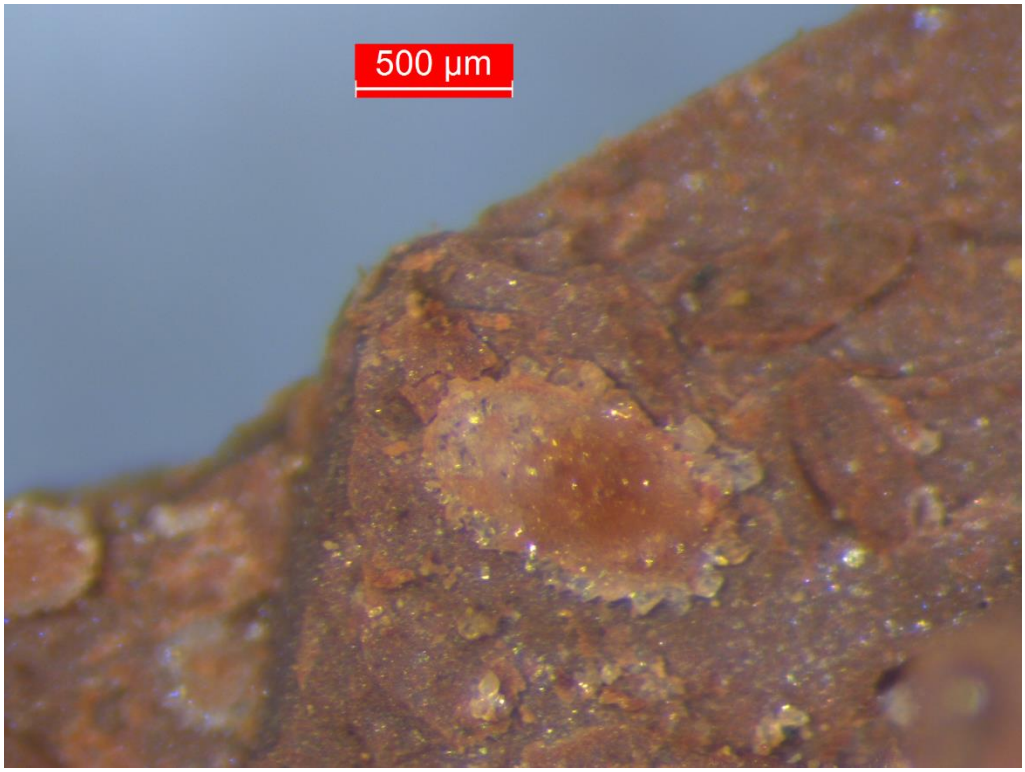

Whitmore Point Reference Section (Potter Canyon, AZ) stable isotope data. n = no value; s = shale; si = siltstone; vfss = very fine sandstone; ms = mudstone

Sample	**Location**	**$\delta^{13}C$ Organic (VPDB)**	**$\delta^{13}C$ Carbonate (VPDB)**	**fractionation $\delta^{13}C$**	**$\delta^{18}O$ Carbonate (VSMOW)**	**$\delta^{18}O$ Carbonate (VPDB)**	**Relative Organic Carbon (%)**	**CO_3 lost (%)**	**Rock Type**
WPRS 1	2.6	-24.08	-4.26	-19.82	28.53	-2.31	0.050	13.7432	s
WPRS 2	5.41	-25.10	-2.84	-22.26	33.06	2.08	0.066	13.0305	si
WPRS 3	5.95	-24.01	-2.80	-21.21	28.56	-2.27	0.038	14.7947	s
WPRS 4	6.74	-25.35	-3.81	-21.54	27.06	-3.73	0.038	14.638	vfss
WPRS 4.5	8.15	-25.44	-3.98	-21.45	25.47	-5.28	0.080	20.0708	si
WPRS 5	9.86	-25.45	-3.65	-21.80	27.26	-3.54	0.046	21.2691	s
WPRS 6	10.185	-30.09	-5.28	-24.81	30.59	-0.31	0.307	32.1396	s
WPRS 7	10.6	-30.26	-5.73	-24.54	31.15	0.24	0.291	26.5283	s
WPRS 8	11.06	-26.89	-6.77	-20.12	30.42	-0.47	0.283	85.8196	stromatolite
WPRS 9	11.29	-27.07	-6.30	-20.77	30.32	-0.57	0.234	33.6849	ms
WPRS 10	11.57	-24.14	-4.46	-19.68	30.32	-0.57	0.103	9.3358	s
WPRS 11	11.96	-23.67	-6.45	-17.23	32.53	1.57	0.066	19.5942	vfss
WPRS 12	12.11	-23.30	-5.70	-17.60	30.46	-0.43	0.072	40.7331	s

Whitmore Point Reference Section (Potter Canyon, AZ) stable isotope data. n = no value; s = shale; si = siltstone; vfss = very fine sandstone; ms = mudstone

Sample	**Location**	**$\delta^{13}C$ Organic (VPDB)**	**$\delta^{13}C$ Carbonate (VPDB)**	**fractionation $\delta^{13}C$**	**$\delta^{18}O$ Carbonate (VSMOW)**	**$\delta^{18}O$ Carbonate (VPDB)**	**Relative Organic Carbon (%)**	**CO_3 lost (%)**	**Rock Type**
WPRS 13	12.305	-24.06	-5.12	-18.94	21.85	-8.79	0.024	8.5545	s
WPRS 14	12.92	-23.22	-3.30	-19.92	33.94	2.94	0.029	4.7803	s
WPRS 15	13.36	-24.17	-4.24	-19.93	25.95	-4.80	0.056	30.5442	vfss
WPRS 16	13.95	-23.43	-2.77	-20.65	30.78	-0.13	0.053	26.4426	ms
WPRS 17	14.66	-24.14	-4.40	-19.73	23.61	-7.07	0.026	33.9883	ms
WPRS 18	15.345	-25.28	-3.10	-22.18	29.86	-1.01	0.037	20.972	ms
WPRS 19	16.49	-24.82	-3.87	-20.95	26.00	-4.76	0.040	10.3956	ms
WPRS 20	17.42	-25.09	-4.96	-20.12	30.43	-0.47	0.028	11.2991	ms
WPRS 21	18.89	-25.65	-4.24	-21.41	37.65	6.54	n	10.6401	ms
WPRS 22	19.31	-24.51	-6.24	-18.27	35.37	4.33	0.032	13.0596	si
WPRS 23	19.8	-24.34	-5.15	-19.20	32.63	1.67	0.033	20.349	si
WPRS 24	20.25	-24.84	-4.59	-20.25	33.68	2.69	0.048	16.5532	ms
WPRS 25	21.12	-25.55	-5.21	-20.34	26.19	-4.58	0.035	24.9778	si

Whitmore Point Reference Section (Potter Canyon, AZ) stable isotope data. n = no value; s = shale; si = siltstone; vfss = very fine sandstone; ms = mudstone

Sample	**Location**	**$\delta^{13}C$ Organic (VPDB)**	**$\delta^{13}C$ Carbonate (VPDB)**	**fractionation $\delta^{13}C$**	**$\delta^{18}O$ Carbonate (VSMOW)**	**$\delta^{18}O$ Carbonate (VPDB)**	**Relative Organic Carbon (%)**	**CO_3 lost (%)**	**Rock Type**
WPRS 26	21.97	-25.98	-6.10	-19.88	28.58	-2.25	0.099	45.35	si
WPRS 27	22.25	-26.19	-5.71	-20.48	28.55	-2.29	0.065	33.3998	si
WPRS 28	22.59	-25.62	-6.26	-19.36	30.63	-0.27	0.040	22.9145	s
WPRS 29	22.96	-25.91	-6.46	-19.45	30.41	-0.48	0.057	27.0781	s
WPRS 30	23.2	-26.01	-6.17	-19.84	29.74	-1.13	0.047	29.9588	s
WPRS 31	23.33	-26.23	-5.98	-20.25	29.82	-1.06	0.051	40.1879	si
WPRS 32	23.91	-25.69	-5.86	-19.83	27.62	-3.19	0.032	11.0156	s
WPRS 33	24.66	-26.10	-6.46	-19.64	32.79	1.82	0.056	45.9213	s
WPRS 34	25.07	-25.89	-6.97	-18.91	33.48	2.49	0.089	44.5433	s
WPRS 35	25.5	-26.06	-6.97	-19.08	31.40	0.48	0.048	32.3118	si
WPRS 36	26.44	-25.62	-5.58	-20.05	27.33	-3.47	0.041	36.6263	ms

Warner Valley, UT stable isotope data. s = shale; si = siltstone; vfss = very fine sandstone; ms = mudstone

Sample	**Location**	**$\delta^{13}C$ Organic (VPDB)**	**Relative Organic Carbon (%)**	**CO_3 lost (%)**	**Rock Type**
WPM-WV 1	31.5	-28.41	0.094	19.46	vfss
WPM-WV 2	63	-28.22	0.046	25.90	vfss
WPM-WV 3	94.5	-27.71	0.071	22.99	si
WPM-WV 4	126	-28.46	0.091	16.88	si
WPM-WV 5	157.5	-28.05	0.111	23.23	si
WPM-WV 6	187.5	-26.94	0.031	27.76	vfss
WPM-WV 7	217.5	-27.55	0.063	28.67	vfss
WPM-WV 8	247.5	-27.94	0.054	24.08	si
WPM-WV 9	277.5	-27.67	0.055	31.65	vfss
WPM-WV 11	337.5	-27.62	0.041	29.02	vfss
WPM-WV 12	367.5	-27.68	0.064	31.48	vfss
WPM-WV 13	397.5	-28.21	0.049	29.88	vfss
WPM-WV 14	427.5	-27.69	0.088	20.71	vfss
WPM-WV 15	457.5	-28.30	0.111	36.72	vfss
WPM-WV 16	487.5	-24.37	0.026	36.12	si
WPM-WV 17	517.5	-26.64	0.047	38.26	si
WPM-WV 18	547.5	-25.42	0.025	40.64	si
WPM-WV 19	577.5	-26.64	0.083	31.74	si
WPM-WV 20	607.5	-26.81	0.081	42.32	si

Warner Valley, UT stable isotope data. s = shale; si = siltstone; vfss = very fine sandstone; ms = mudstone (cont.)

Sample	Location	$\delta^{13}C$ Organic (VPDB)	Relative Organic Carbon (%)	CO_3 lost (%)	Rock Type
WPM-WV 21	637.5	-27.02	0.087	36.84	si
WPM-WV 22	667.5	-27.01	0.067	33.37	si
WPM-WV 23	697.5	-24.40	0.056	39.54	vfss
WPM-WV 24	757.5	-26.91	0.041	27.24	s
WPM-WV 25	787.5	-27.60	0.079	13.18	vfss
WPM-WV 26	817.5	-28.32	0.075	24.95	ms
WPM-WV 27	847.5	-27.76	0.055	19.33	s
WPM-WV 28	877.5	-26.95	0.073	11.12	s
WPM-WV 29	907.5	-27.69	0.056	18.81	s
WPM-WV 30	937.5	-27.43	0.057	18.39	vfss
WPM-WV 31	967.5	-27.99	0.043	24.74	vfss
WPM-WV 32	997.5	-28.72	0.127	34.00	ms
WPM-WV 33	1027.5	-28.42	0.107	26.80	ms
WPM-WV 34	1057.5	-26.58	0.044	28.46	ms
WPM-WV 35	1087.5	-27.68	0.079	36.81	si
WPM-WV 36	1117.5	-28.18	0.115	26.87	s
WPM-WV 37	1147.5	-26.46	0.045	35.33	ms
WPM-WV 38	1177.5	-28.54	0.125	33.07	si
WPM-WV 39	1207.5	-25.96	0.117	30.97	ms

Warner Valley, UT stable isotope data. s = shale; si = siltstone; vfss = very fine sandstone; ms = mudstone (cont.)

Sample	**Location**	**$\delta^{13}C$ Organic (VPDB)**	**Relative Organic Carbon (%)**	**CO_3 lost (%)**	**Rock Type**
WPM-WV 39 M	1207.5	-26.68	0.108	12.10	ms
WPM-WV 40	1237.5	-25.64	0.040	50.48	ms
WPM-WV 41	1267.5	-26.64	0.066	25.30	s
WPM-WV 42	1297.5	-23.97	0.122	35.53	ms
WPM-WV 43 G	1327.5	-28.54	0.146	45.79	ms
WPM-WV 44 G	1357.5	-28.58	0.139	56.12	ms
WPM-WV 45	1387.5	-26.20	0.060	61.55	s
WPM-WV 46	1417.5	-26.88	0.066	7.49	s
WPM-WV 47	1447.5	-26.02	0.040	12.77	si
WPM-WV 48	1467.5	-24.60	0.038	25.27	si
WPM-WV 49 M	1482.5	-27.10	0.070	19.63	ms
WPM-WV 55	1502.5	-26.65	0.117	58.03	vfss
WPM-WV 50 M	1512.5	-27.79	0.087	41.38	s
WPM-WV 51	1542.5	-28.19	0.092	48.76	si
WPM-WV 52	1572.5	-25.24	0.026	28.49	vfss
WPM-WV 53	1602.5	-25.64	0.029	29.63	vfss
WPM-WV 54	1632.5	-25.10	0.026	22.78	s

Potter Canyon sample locations and units. See Kirkland et al., 2014 for unit descriptions.

Sample	Sample Location	Strat. Unit #	Unit Thickness	Running Thickness
WPRS 1	2.6	0	292	260
WPRS 2	5.41	3	6	541
WPRS 3	5.95	5	7	595
WPRS 4	6.74	10	26	674
WPRS 4.5	8.15	13	110	815
WPRS 5	9.86	18	24	986
WPRS 6	10.185	20	86	1018.5
WPRS 7	10.6	20	86	1060
WPRS 8	11.06	21	3	1106
WPRS 9	11.29	23	10	1129
WPRS 10	11.57	24	61	1157
WPRS 11	11.96	25	11	1196
WPRS 12	12.11	27	2	1211
WPRS 13	12.305	28	80	1230.5
WPRS 14	12.92	28	80	1292
WPRS 15	13.36	31	24	1336
WPRS 16	13.95	33	64	1395
WPRS 17	14.66	36	11	1466
WPRS 18	15.345	38	33	1534.5
WPRS 19	16.49	40	98	1649

Potter Canyon sample locations and units. See Kirkland et al., 2014 for unit descriptions.

Sample	Sample Location	Strat. Unit #	Unit Thickness	Running Thickness
WPRS 20	17.42	42	70	1742
WPRS 21	18.89	45	13	1889
WPRS 22	19.31	48	14	1931
WPRS 23	19.8	50	45	1980
WPRS 24	20.25	52	28	2025
WPRS 25	21.12	54	58	2112
WPRS 26	21.97	57	48	2197
WPRS 27	22.25	57	48	2225
WPRS 28	22.59	60	12	2259
WPRS 29	22.96	63	31	2296
WPRS 30	23.2	64	31	2320
WPRS 31	23.33	64	31	2333
WPRS 32	23.91	66	35	2391
WPRS 33	24.66	70	18	2466
WPRS 34	25.07	73	14	2507
WPRS 35	25.5	76	18	2550
WPRS 36	25.44	80	15	2544

Warner Valley sample locations and sample description.

Sample	Description	Location (cm)	Interval (cm)	Notes
WPM-WV 1	red brown vfss with fine bedding (laminae); right above contact w gray (bleached) s.s.; muddy?	31.5	31.5	
WPM-WV 2	vfss to pale gray/green with red muddy/clay layers; darker green clay layer	63	31.5	
WPM-WV 3	dark brown with light gray layers; fine x bedding silty w/mud (siltstone) possible ostracods and conchostracans	94.5	31.5	
WPM-WV 4	dark brown; gritty; mudstone or siltstone; layered very finely	126	31.5	
WPM-WV 5	dark reddish brown; sandy mudstone with some coarse grains; not a distinct bedding	157.5	31.5	
WPM-WV 6	bownish red; vfss; possible ostracods about ten centimeters above contact with muddy silty mudstone	187.5	30	
WPM-WV 7	red vfss with some mud; very fine beds looks like it contains soom carbonate strom (very thin)	217.5	30	looks like this sample contains a contact
WPM-WV 8	mddy ss with carbonate layers (stromatolites) micro mudcracks fine bedding	247.5	30	
WPM-WV 9	vfss with bedding; brown red color; may contain some carb	277.5	30	
WPM-WV 10	muddy ss with potential ostrcaods; red to grey	307.5	30	
WPM-WV 11	fine sandy mudstone possible conchostracans and ostracods reddish grey color	337.5	30	*sighted out wpm wv 11 on new outcrop. End @ 3:00
WPM-WV 12	vfss; slight ripple thin bed; pinches out laterally; reddish brown no acid rxn	367.5	30	
WPM-WV 13	vfss to siltsone; thin layers, no acid rxn; reddish brown	397.5	30	
WPM-WV Carb 1	below (1-3 cm) sample 13 looks like travertine; is a carbonate (reacts with acid) Oncolite look to it; possibly anhydrite replaced by calcite or surficial weathering	395.5	-2	

Warner Valley sample locations and sample descriptions.

Sample	Description	Location (cm)	Interval (cm)	Notes
WPM-WV 14	followed carb. Layer around wash to Jim's old trench looks to very brittle very fine s.s. to siltstone with clay partings (bedded) reddish	427.5	30	30 above wpm-wv 13
WPM-WV 15	vfss to white/pale white mottles; burrows; slight effervescence (CaCO3 cement)	457.5	30	
WPM-WV 16	calcareous siltstone (very fine grained) reddish brown with ~2mm diameter mottles; slight effervescence	487.5	30	
WPM-WV 17	siltstone pale green with red mottles; effervescence (10 cm thick)	517.5	30	
WPM-WV 18	red-brown silty mudstone not really gritted; calcareous effervescence; weathers in a blocky pattern	547.5	30	
WPM-WV 19	reddish brown silty mudstone slight horizontal bedding; muddy; kind of shaley some clay; maybe ostracods	577.5	30	
WPM-WV 20	calcareous siltstone with some vfs; fizzes pale red/brown with pale green mottles	607.5	30	
WPM-WV 21	calcareous siltstone with some vfs reddish brown not underated traced bed along ridge to Jim's 7; few cm above sample 21 are mudcracks	637.5	30	
WPM-WV 22	pale red brown; indurated; siltstone with vfs calcareous	667.5	30	
WPM-WV 23	pale green/whitish siltstone with vfs grains; calcareous bleached	697.5	30	
WPM-WV 24	shot @ 60 cm above sample 23 to avoid vegetation and cover light green muddy s.s. with green clay clast! Some red mottles effervescent with HCl	757.5	60	
WPM-WV 25	pale reddish brown, blocky, vfss, some effervescent; pale green mottle	787.5	30	
WPM-WV 26	silty to sandy mudstone brownish/light red pale green mottles no effervescence	817.5	30	

Warner Valley sample locations and descriptions

Sample	Description	Location (cm)	Interval (cm)	Notes
WPM-WV 27	red brown shale with ostracods and conchostracans; fizzy esp on cods not so much matrix	847.5	30	
WPM-WV 28	red brown shale ostracods; slicken slides less bedded more blocky; clay only cods are calcareous	877.5	30	
WPM-WV 29	reddish shale (clay) conchostracans ostracods; no fizz on matrix fizz on cods	907.5	30	
WPM-WV 30	siltstone to vfss no fizz; nodular (may be ripples)	937.5	30	
WPM-WV 31	indurated; pale green vfss; ripples and cross beds	967.5	30	
WPM-WV 32	moved over 3m left of sampling site followed key bed, few cm above WV 31; silty m.s.; blocky; green mottles; no fizz red brown color	997.5	30	
WPM-WV 33	red/brown silty mudstone; blocky; green mottles; blocky no fizz	1027.5	30	
WPM-WV 34	red/brown silty ms with more silt; green mottles; no fizz	1057.5	30	
WPM-WV 35	sample is right @ boundary btw silty ms and green bed. Green is more resistant siltstone	1087.5	30	
WPM-WV 36	calcareous shale no grit; surficial salt (gypsum?) reddish brown; clayey	1117.5	30	
WPM-WV 37	red brown silty ms no fizz; blocky/nodular cleavage	1147.5	30	
WPM-WV 38	at top of green indurated layer (6 cm thick layer) siltstone; calcareous (fizzes); slightly laminated	1177.5	30	
WPM-WV 39	red brown silty ms ; no rxn; surficial calcareous tufa? Calcrete? Caliche? Maybe in place sample taken	1207.5	30	
WPM-WV 40	reddish/brown; greenish gray silty ms laminated, platy, calcareous	1237.5	30	

Warner Valley sample locations and sample descriptions.

Sample	Description	Location (cm)	Interval (cm)	Notes
WPM-WV 40	reddish/brown; greenish gray silty ms laminated, platy, calcareous	1237.5	30	
WPM-WV 41	white buggy carbonate taken inter layered green/red (redoxamorphic) fissile, laminated siltstone, maybe shale	1267.5	30	
WPM-WV 42	white buggy carbonate taken inter layered green/red (redoxamorphic) fissile, laminated siltstone; reaction	1297.5	30	
WPM-WV 43	interlayered redoxamorphic silty ms with vfs more fissile; weakly cemented	1327.5	30	
WPM-WV 44	pale green silty ms. Slight effervescence about 2 cm under contact with red silty ms; red does not fizz crumbly	1357.5	30	
WPM-WV 45	interbedded redoxamorphic (mostly red) silty ms blocky more rxn than wpm wv 44; red layer does not fizz; green does; picture on Daigo's phone	1387.5	30	
WPM-WV 46	gray, green, red, yellow very fissile/crumbly clayey ms no rxn with HCl; shaley (fissile) kind of platy blocky breakage	1417.5	30	
WPM-WV 47	moved to vertical outcrop using yellow banded layer as guide; yellow siltstone, nodular green mottles react with HCl	1447.5	30	
WPM-WV 48	red/brown blocky silty ms green mottled no HCl rxn well cemented/indurated coarsening upward from yellow layer to base of stomatolite	1467.5	30	
WPM-WV 49	stromatolites thin layer; fragileno apparent HCl rxn; Dolomite?; above green ms reacts; carbonaceous calcretes? Above below and in stromatolites react with acid	1482.5	30	
WPM-WV 50	well cemented shale with buggy carbonate, nodulaes (rhizocretes) nodules sampled and matrix sampled green mottles sampled	1512.5	30	
	green mottles; possible burrows or root traces; picture #5 Daigo's phone		30	
WPM-WV 51	redoxamorphic measured into green layer (reduced) siltstone; well cemented slightly calcareous	1542.5	30	

Warner Valley sample locations and sample descriptions.

Sample	**Description**	**Location (cm)**	**Interval (cm)**	**Notes**
WPM-WV 52	brown fine ss; laminated; moderate sedimentation; green mottles no rxn	1572.5	30	
WPM-WV 53	reddish brown with larger green mottles; vfss; laminated	1602.5	30	
WPM-WV 54	green shaley siltstone right below contact with Kayenta Fm slight HCl RXN	1632.5	30	
WPM-WV 55	vfss with cods; conchostracans and fish debris		+ 20 above stromatolite layer	

Warner Valley stratigraphic section. See Kirkland et al., 2014 for Potter Canyon stratigraphic section.